Published OnlineFirst September 30, 2013; DOI: 10.1158/1078-0432.CCR-13-0742

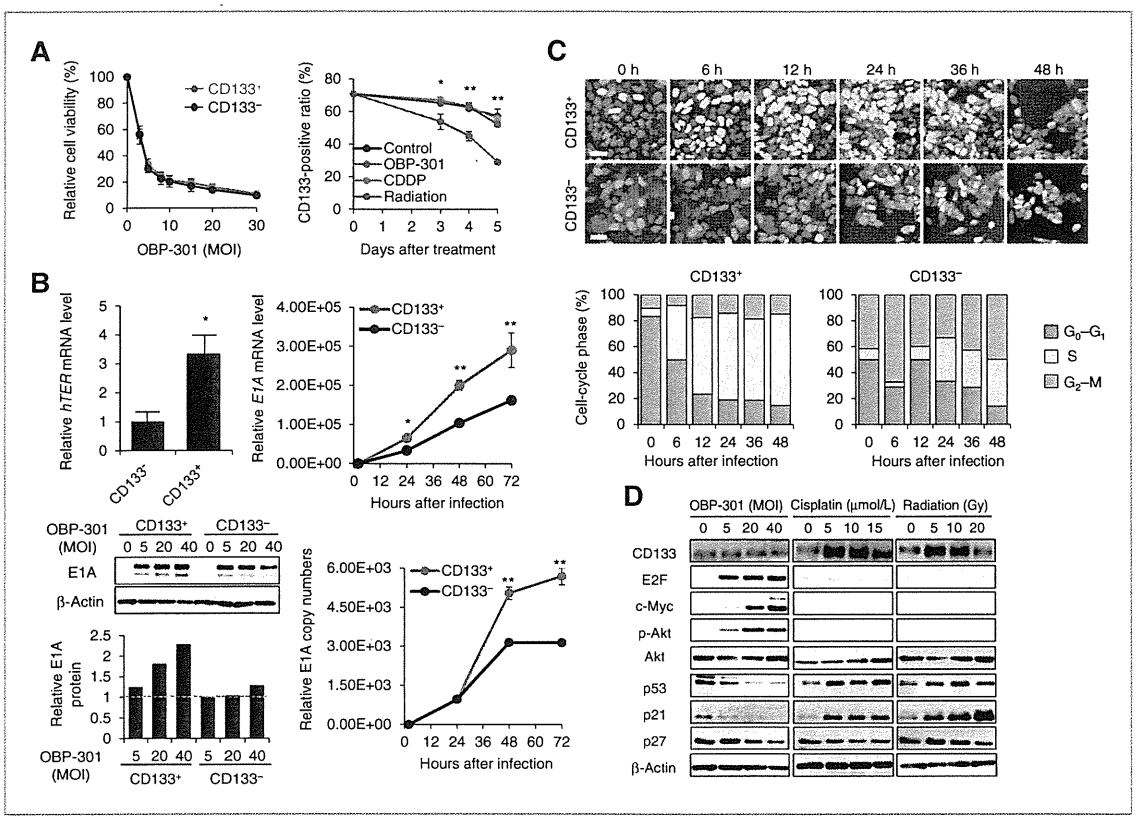

Figure 2. OBP-301 lethally induces S-phase transition of quiescent CD133$^+$ cancer stem–like cells and decreases cancer stem–like cell frequency via enhanced viral replication. A, OBP-301 efficiently kills CD133$^+$ cancer stem–like cells. Left, viability of CD133$^+$ and CD133$^-$ MKN45 cells after OBP-301 infection. Right, CD133-positive ratio of MKN45 cells treated with OBP-301, cisplatin, or radiation was analyzed by flow cytometry. B, OBP-301 can replicate more in CD133$^+$ cells that have more hTERT activity than in CD133$^-$ cells. Expression of *hTERT* mRNA in CD133$^+$ and CD133$^-$ MKN45 cells assessed by qRT-PCR (top left). The relative levels of *hTERT* mRNA were calculated after normalization with reference to the expression of *PBGD* mRNA. Expression of *E1A* mRNA in CD133$^+$ and CD133$^-$ MKN45 cells after OBP-301 infection at an MOI of 10 PFU/cell for 2 hours. Expression of *E1A* mRNA was analyzed over the following 3 days by qRT-PCR (top right). The relative levels of *E1A* mRNA were calculated after normalization with reference to the expression of *GAPDH* mRNA. Western blot analysis of E1A expression in CD133$^+$ and CD133$^-$ MKN45 cells treated with OBP-301 for 48 hours (bottom left). Quantitative relative expression level of E1A protein, normalized to β-actin, using NIH ImageJ software (bottom left). Quantitative measurement of viral DNA replication in CD133$^+$ and CD133$^-$ MKN45 cells after OBP-301 infection at an MOI of 10 PFU/cell for 2 hours (bottom right). *E1A* copy number was analyzed over the following 3 days using qPCR. C, time-lapse imaging of FUCCI-expressing CD133$^+$ and CD133$^-$ cells treated with OBP-301 at an MOI of 20 PFU/cell. The cells in G_0–G_1, S, or G_2–M phases appear red, yellow, or green, respectively. Histogram shows the cell-cycle phases of FUCCI-expressing CD133$^+$ and CD133$^-$ cells treated with OBP-301 for 48 hours. The percentage of cells in G_0–G_1, S, and G_2–M phases are shown. D, Western blot analysis of E2F1, c-Myc, phospho-Akt, Akt, p53, p21, and p27 expression in CD133$^+$ cells treated with OBP-301, cisplatin, or radiation for 48 hours. β-Actin was assayed as a loading control for all experiments. Data are shown as means ± SD ($n = 5$). *, $P < 0.05$; **, $P < 0.01$.

cell-cycle accelerators (27) and decreased the expression of p53, p21, and p27 proteins that function as cell-cycle brakes (27) in quiescent CD133$^+$ cells (Fig. 2D). In contrast, cisplatin and radiation increased the expression of p53 and p21 proteins (Fig. 2D). We further examined whether adenoviral E1A altered the expression of these proteins in CD133$^+$ cells. E1A-expressing OBP-301 and Ad5, but not E1A-defficient dl312, similarly altered the expression of these proteins in CD133$^+$ cells (Supplementary Fig. S9). These results indicate that OBP-301 induces cell-cycle progression through upregulation of E2F-related proteins and downregulation of p53-related and p27 proteins by enhanced adenoviral E1A in quiescent cancer stem–like cells.

Three-dimensional tumor spheres maintain a CD133$^+$ subpopulation by remaining quiescent

Formation of tumor spheres under serum-free conditions is frequently used to maintain cancer stem–like cell subpopulations (28). The addition of serum makes floating undifferentiated tumor spheres adherent and their cells differentiate into adherent cells (29). Therefore, we hypothesized that tumor spheres maintained their cancer stem–like cell frequency due to quiescence.

Published OnlineFirst September 30, 2013; DOI: 10.1158/1078-0432.CCR-13-0742

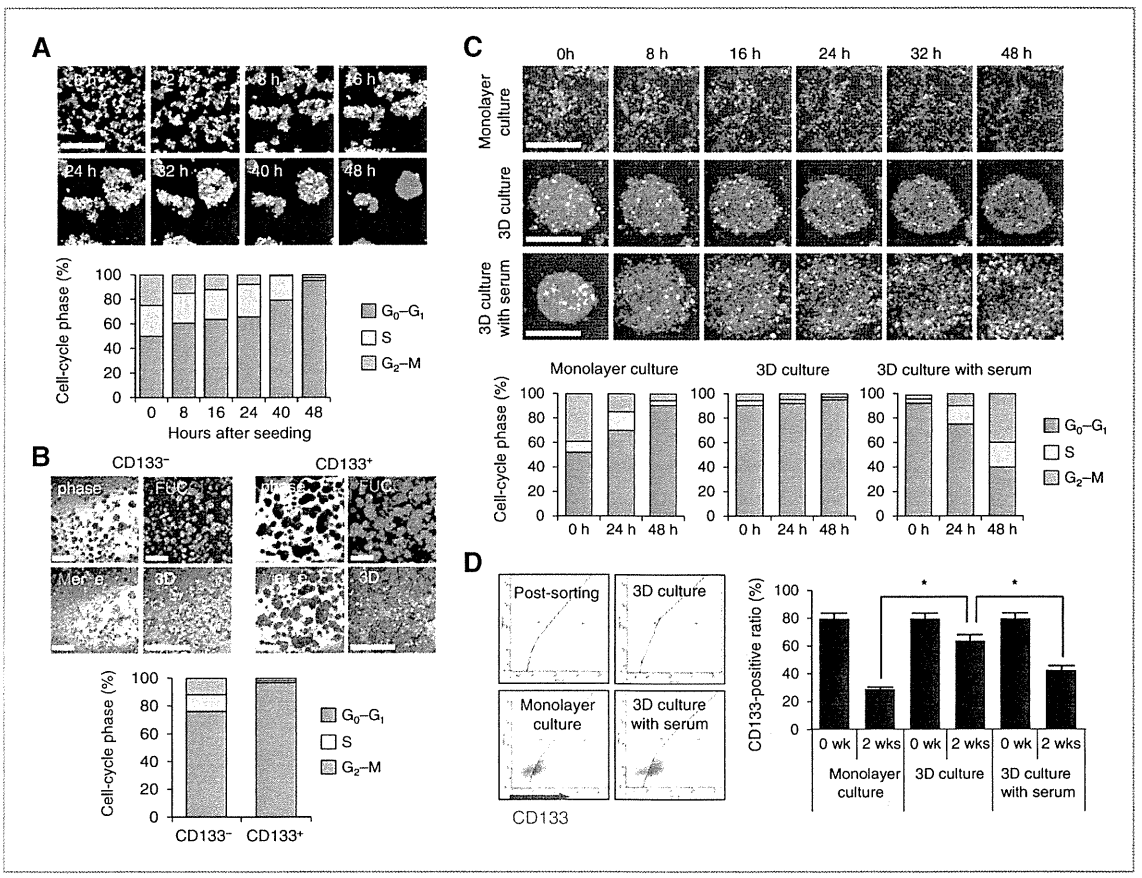

Figure 3. Three-dimensional tumor spheres maintain $CD133^+$ cells by the cell cycle arrest. A, time-lapse images of FUCCI-expressing $CD133^+$ cells in 3-dimensional culture without serum. Purified FUCCI-expressing $CD133^+$ cells were cultured on agar in serum-free medium containing EGF and bFGF for 48 hours (top). The cells in G_0–G_1, S, or G_2–M phases appear red, yellow, or green, respectively. Histogram shows the cell-cycle phase of FUCCI-expressing $CD133^+$ cells in 3-dimensional culture without serum (bottom). The percentage of cells in G_0–G_1, S, and G_2–M phases are shown. B, representative images of tumor spheres formed from FUCCI-expressing $CD133^+$ and $CD133^-$ cells (top). Histogram shows the cell-cycle phase of tumor spheres from FUCCI-expressing $CD133^+$ and $CD133^-$ cells (bottom). C, time-lapse images of FUCCI-expressing $CD133^+$ cells in monolayer culture or FUCCI-expressing tumor spheres in 3-dimensional culture without serum (3D without serum) or tumor spheres in monolayer culture with serum (monolayer culture; top). Histogram shows the cell-cycle phase of FUCCI-expressing $CD133^+$ cells in 2D culture, FUCCI-expressing established tumor spheres in 3D without serum, or tumor spheres on plastic culture with serum (monolayer culture; bottom). D, comparison of changes in the $CD133^+$-positive ratio in monolayer culture, tumor spheres in 3D culture without serum, or with serum. Representative dot plots (left) and data from 3 experiments (right) are shown. Data are shown as means ± SD ($n = 5$). *, $P < 0.01$. Scale bars, 500 μm.

$CD133^+$ cells aggregated and formed tumor spheres, and arrested in G_0–G_1 phase (Fig. 3A). Tumor spheres formed from $CD133^+$ cells contained more quiescent cells than those formed from $CD133^-$ cells (Fig. 3B). Moreover, established tumor spheres formed from $CD133^+$ cells remained quiescent in 3-dimensional culture without serum (Fig. 3C). In contrast, established tumor spheres, after addition of serum, exited from the quiescent state and began to cycle, divide, and increase (Fig. 3C and Supplementary Movie S2). Flow cytometric analysis showed that $CD133^+$ cells could be maintained in tumor spheres cultured in serum-free medium for 2 weeks, whereas the percentage of $CD133^+$ cells significantly decreased in monolayer cultures or in tumor spheres cultured in serum-containing medium (Fig. 3D). These data indicate that tumor spheres maintain their cancer stem-cell frequency by remaining dormant.

Real-time imaging spatiotemporally shows OBP-301 eliminates dormant tumor spheres by cell-cycle mobilization and S/G_2/M phase trapping

To further evaluate OBP-301-induced cell-cycle mobilization and S-phase trapping in dormant tumor spheres, we visualized the treatment dynamics of FUCCI-expressing tumor spheres infected with OBP-301. Time-lapse imaging showed that OBP-301 infected quiescent $CD133^+$ cells at the periphery of the spheres and then induced S and G_2–M

Published OnlineFirst September 30, 2013; DOI: 10.1158/1078-0432.CCR-13-0742

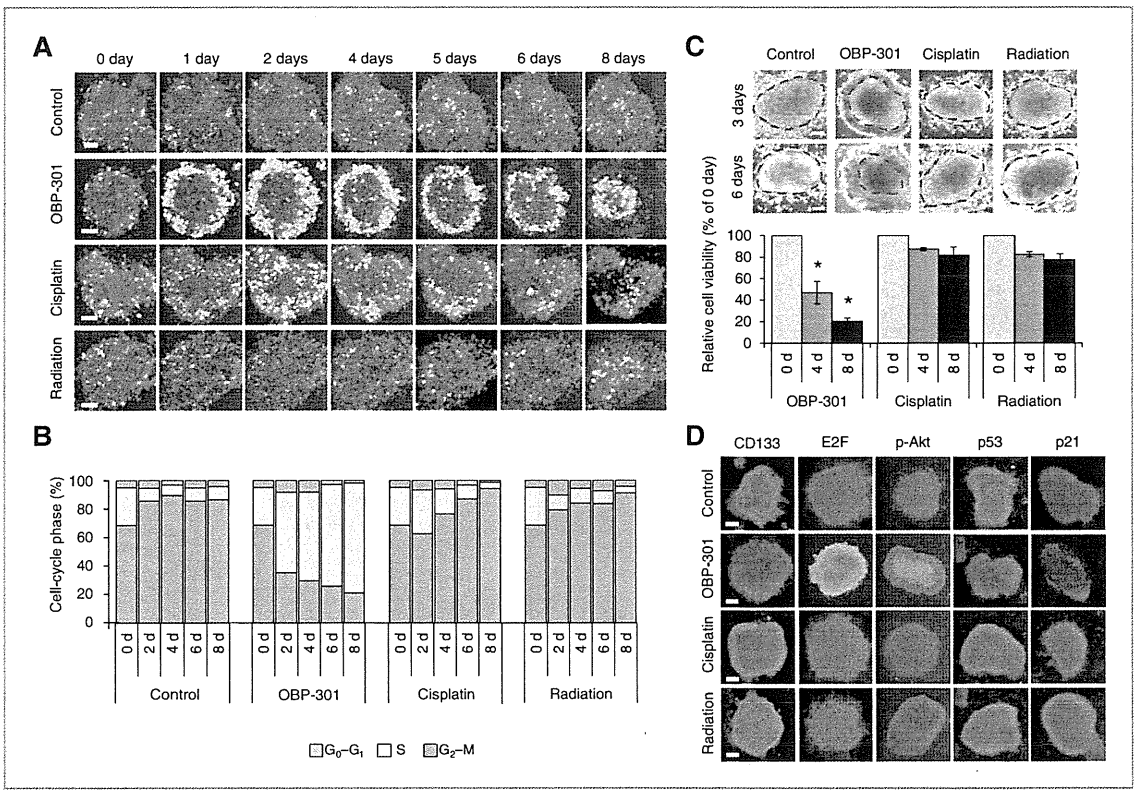

Figure 4. Visualization of elimination of dormant tumor spheres by virus infection. A, time-lapse images of tumor spheres treated with OBP-301 (5×10^6 PFU), cisplatin (10 μmol/L), or radiation (10 Gy). The cells in G_0–G_1, S, or G_2–M phases appear red, yellow, or green, respectively. B, histogram shows the cell-cycle phases of the spheres with OBP-301, cisplatin, or radiation. The percentage of cells in G_0–G_1, S, and G_2–M phases are shown. C, representative images of control, OBP-301-, cisplatin-, or radiation-treated spheres (top). Histogram shows the relative cell viability of treated tumor spheres (bottom). D, the $CD133^+$ tumor spheres treated as above were stained for E2F1, phospho-Akt, p53, and p21. Immuofluorescence staining was visualized by confocal laser microscopy. Scale bars, 100 μm. Data are shown as means ± SD ($n = 5$). *, $P < 0.01$.

phase entry, leading to cellular death by viral replication (Fig. 4A). Moreover, as OBP-301 penetrated into the deeper layers, tumor spheres gradually shrunk after virus infection (Fig. 4A and C). In contrast, cisplatin and radiation did not affect the cell-cycle phase or the size of tumor spheres (Figs. 4A–C and Supplementary Movie S3). Immunofluorescence staining of tumor spheres also confirmed that OBP-301 infection downregulated CD133, p53, and p21 expression and upregulated E2F1 and phospho-Akt expression in tumor spheres (Fig. 4D). These results suggest that OBP-301 efficiently eradicates dormant tumor spheres resistant to conventional therapies by mobilizing them into an $S/G_2/M$ phase trap.

OBP-301 efficiently kills dormant cancer stem–like cells in established human tumor xenografts by cell-cycle mobilization and $S/G_2/M$ phase trapping, thereby reducing cancer stem–like cell frequency

To further confirm whether OBP-301 efficiently reduced $CD133^+$ cancer stem–like cell frequency within tumor tissues (Supplementary Fig. S10A), we investigated the expression of *CD133* mRNA and the CD133-positive ratio in subcutaneous tumors derived from radioresistant MKN45 cells after treatment of OBP-301, cisplatin, or irradiation. Suppression of tumor growth by OBP-301 (Fig. 5A) was accompanied by a significant decrease in *CD133* mRNA at 2 weeks after the final treatment (Fig. 5B). In contrast, although cisplatin and radiation also suppressed tumor growth to a similar extent as OBP-301 (Fig. 5A), cisplatin did not affect, and radiation significantly increased *CD133* mRNA expression at 1 week after the final treatment (Fig. 5B). Immunohistochemistry of CD133-stained tumor sections also showed that OBP-301 reduced the frequency of $CD133^+$ cells, whereas cisplatin and irradiation increased the frequency compared with control (Fig. 5B).

Next, we visualized treatment dynamics in established FUCCI-expressing MKN45 tumor xenografts with or without OBP-301 infection (Supplementary Fig. S10B). FUCCI-expressing MKN45 tumors had a distribution of cancer cells in G_0–G_1, S, and G_2–M phases (Fig. 5A). As tumors grew bigger, cancer cells in G_0–G_1 phase increased (Fig. 5C and D), indicating the existence of dormant cancer cells.

Published OnlineFirst September 30, 2013; DOI: 10.1158/1078-0432.CCR-13-0742

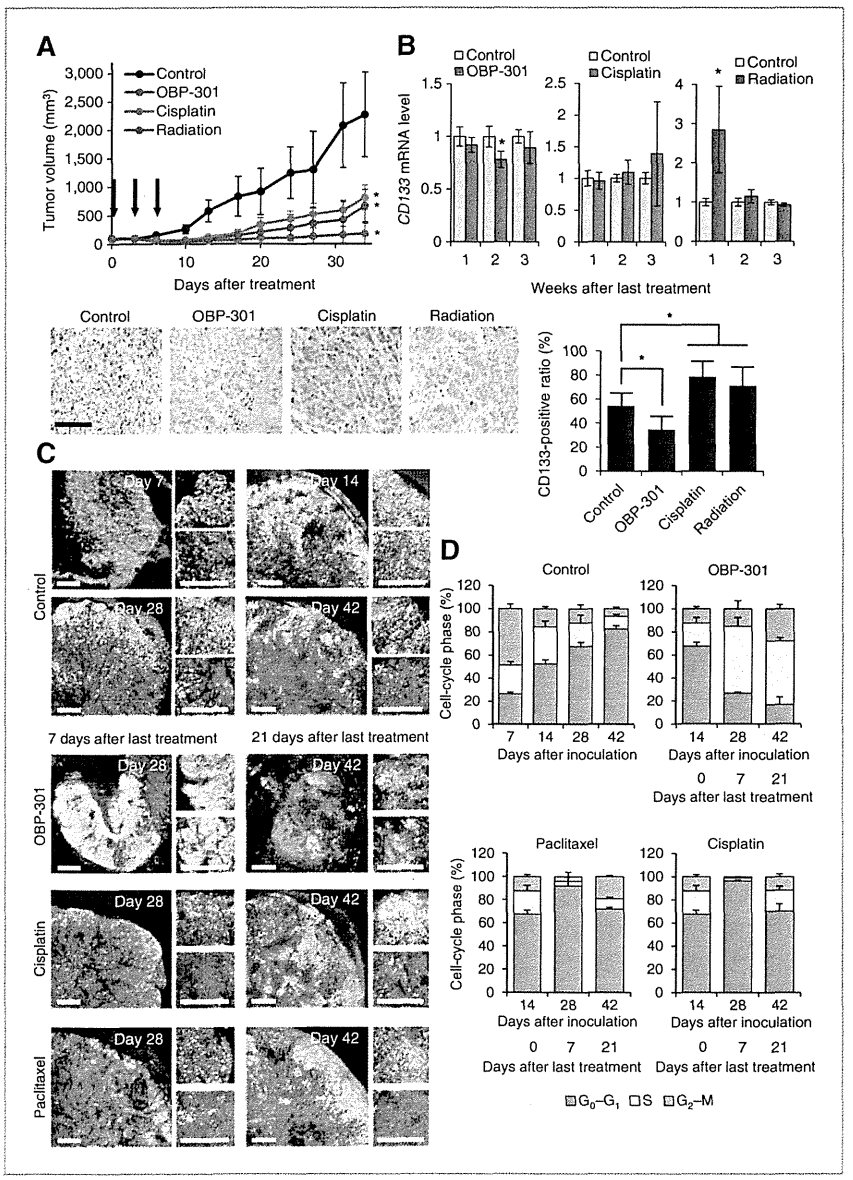

Figure 5. OBP-301 induces cell-cycle progression and efficiently kills dormant cancer cells resistant to conventional therapy in established human tumor xenografts. $CD133^+$-rich radioresistant MKN45 cells (5×10^6 cells/mouse) were injected subcutaneously into the left flanks of mice. When the tumors reached approximately 6 mm in diameter (tumor volume, 100–120 mm^3), mice were administered OBP-301 intratumorally (1×10^8 PFU/tumor), injected intraperitoneally with cisplatin (4 mg/kg), or exposed to 2 Gy of radiation for 3 cycles every 3 days. A, growth curves of tumors derived from radioresistant MKN45 cells after treatment with OBP-301, cisplatin or radiation. Black arrows indicate the day of treatment. B, expression of *CD133* mRNA in tumors treated with OBP-301, cisplatin, or radiation at 1, 2, and 3 weeks after treatment (top). Representative images of CD133-stained tumor section treated with OBP-301, cisplatin, or radiation (bottom left). Scale bars, 100 μm. Histogram shows the percentages of $CD133^+$ cells in tumors treated with OBP-301, cisplatin, or radiation (bottom right). The percentage of $CD133^+$ cells was calculated by dividing the number of $CD133^+$ cells by the total number of cells. Data are shown as means ± SD ($n = 3$). *, $P < 0.05$. C and D, FUCCI-expressing MKN45 cells (5×10^6 cells/mouse) were injected subcutaneously into the left flanks of mice. When the tumors reached approximately 7 mm in diameter (tumor volume, 150–180 mm^3), mice were administered OBP-301 intratumorally (1×10^8 PFU/tumor), injected intraperitoneally with cisplatin (4 mg/kg) or paclitaxel (5 mg/kg) for 3 cycles every 3 days. Representative images of cross-sections of FUCCI-expressing MKN45 subcutaneous tumors of control, OBP-301-, cisplatin-, or paclitaxel-treated mice (left). The cells in G_0–G_1, S, or G_2–M phases appear red, yellow, or green, respectively. Histogram shows the cell-cycle phase of FUCCI-expressing MKN45 subcutaneous tumor from control, OBP-301-, cisplatin-, or paclitaxel-treated mice (right). The percentage of cells in G_0–G_1, S, and G_2–M phases are shown. Data are shown as means ± SD ($n = 5$). *, $P < 0.05$. Scale bars, 500 μm.

Published OnlineFirst September 30, 2013; DOI: 10.1158/1078-0432.CCR-13-0742

After cisplatin or paclitaxel treatment, the tumor consisted mostly of red fluorescent cells (Fig. 5D), indicating that the cytotoxic agents killed only cycling cancer cells and had little effect on quiescent dormant cancer cells. These tumors regrew, with the quiescent cells re-entering the cell cycle 21 days after last treatment (Fig. 5D). In contrast, intratumor injection of OBP-301 mobilized the cancer cells into the $S/G_2/M$ phase trap, leading to elimination of cancer cells in $S/G_2/M$ phases (Fig. 5D). These data indicate that OBP-301 could efficiently kill quiescent cancer stem–like cells in tumors by inducing cell-cycle progression.

OBP-301 sensitizes quiescent cancer stem–like cells to chemotherapy by cell-cycle mobilization and $S/G_2/M$ phase trapping

As we previously showed that OBP-301 enhances the sensitivities to chemotherapeutic agents in various types of human cancer cells (30, 31), we further evaluated whether OBP-301 sensitizes quiescent $CD133^+$ cancer stem–like cells to chemotherapy by inducing cell-cycle progression and $S/G_2/M$ phase trapping. OBP-301 infection significantly enhanced the inhibitory effect of chemotherapy on cell viability and tumor sphere formation of $CD133^+$ cells (Fig. 6A and Supplementary

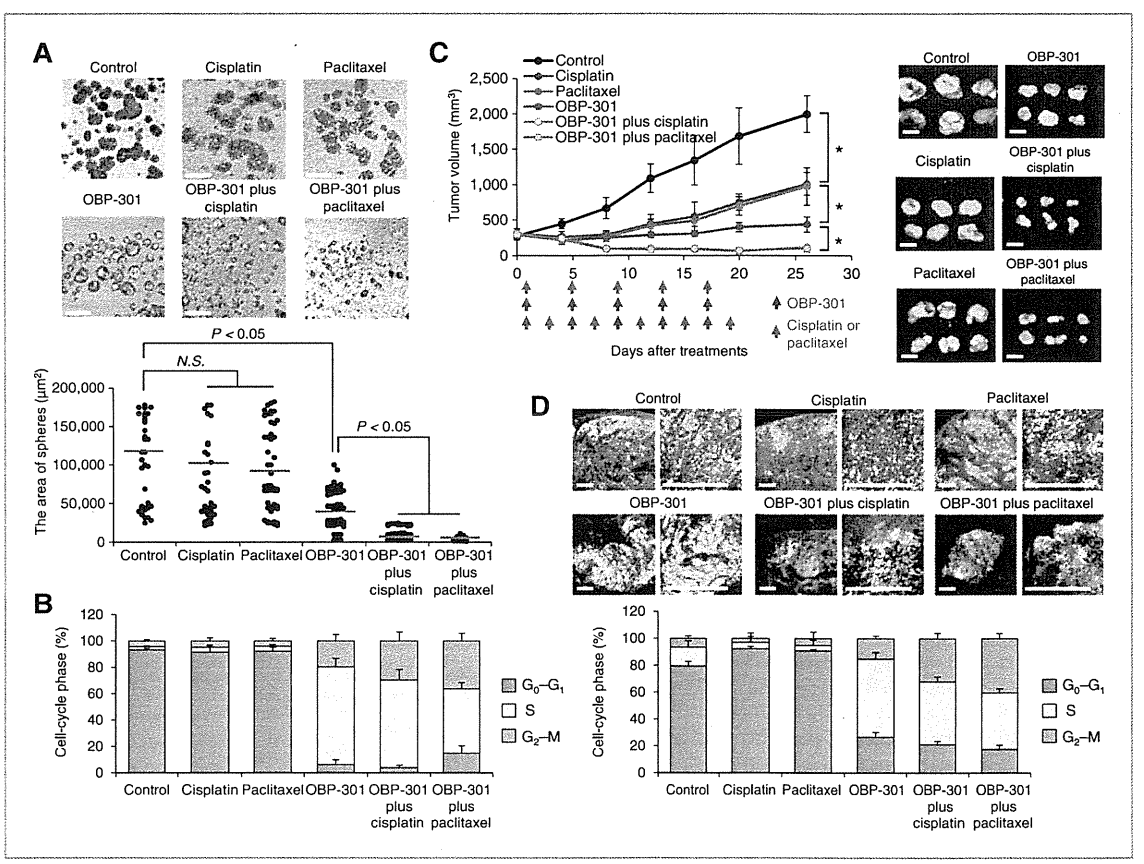

Figure 6. OBP-301 sensitizes quiescent $CD133^+$ cancer stem–like cells to chemotherapy by inducing cell-cycle progression. A, representative images of tumor spheres from FUCCI-expressing $CD133^+$ cells after treatment with cisplatin, paclitaxel, OBP-301, and the combination of OBP-301 and chemotherapy (top). The cells in G_0–G_1, S, or G_2–M phases appear red, yellow, or green, respectively. The tumor-sphere area was calculated using NIH ImageJ software (lower). Data are shown as means ± SD ($n = 5$). *, $P < 0.05$. Scale bars, 500 μm. B, histogram shows the cell-cycle phase of tumor spheres from FUCCI-expressing $CD133^+$ cells after treatment with chemotherapy, OBP-301, and the combination of OBP-301 and chemotherapy. The percentage of cells in G_0–G_1, S, and G_2–M phases are shown. Data are shown as means ± SD ($n = 5$). *, $P < 0.05$. C, FUCCI-expressing MKN45 cells (5×10^6 cells/mouse) were injected subcutaneously into the left flanks of mice. When the tumors reached approximately 8 mm in diameter (tumor volume, 300 mm^3), mice were administered OBP-301 intratumorally (1×10^8 PFU/tumor), injected intraperitoneally with cisplatin (4 mg/kg) or paclitaxel (5 mg/kg) for 5 cycles every 3 days. The growth curves of tumors derived from FUCCI-expressing MKN45 cells after treatment with chemotherapy, OBP-301, or the combination of OBP-301 and chemotherapy (left). Red and green arrows indicate the day of treatment with OBP-301 and chemotherapy, respectively. Macroscopic photographs of FUCCI-expressing tumors in untreated (control) or treated with OBP-301, cisplatin, paclitaxel, or the combination of OBP-301 and chemotherapy (right). Scale bars, 10 mm. D, representative image of cross-sections of FUCCI-expressing MKN45 subcutaneous tumors of control, OBP-301-, cisplatin-, paclitaxel-, or the combination of OBP-301- and chemotherapy-treated mice (top). Histogram shows cell-cycle phase of FUCCI-expressing MKN45 subcutaneous tumors of control, treated with OBP-301, cisplatin, paclitaxel, or the combination of OBP-301 and chemotherapy (bottom). Data are shown as means ± SD ($n = 6$). *, $P < 0.05$, ANOVA. Scale bars, 500 μm.

Published OnlineFirst September 30, 2013; DOI: 10.1158/1078-0432.CCR-13-0742

Fig. S13). Tumor spheres treated with chemotherapy and OBP-301 contained an increased percentage of tumor cells in G_2–M phases compared to OBP-301 alone (Fig. 6B). The combination of OBP-301 and chemotherapy (Supplementary Fig. S10C) significantly suppressed tumor growth compared to chemotherapy or OBP-301 alone (Fig. 6C and Supplementary Fig. S14). Cross-sections of tumor tissues showed that the combination of chemotherapy and OBP-301 induced an increased percentage of cancer cells in G_2–M phases compared to OBP-301 alone (Fig. 6D). These results suggest that OBP-301 sensitizes the quiescent cancer stem–like cells to chemotherapy-mediated G_2–M arrest by inducing cell-cycle progression and S/G_2/M phase trapping.

Discussion

We have described that a bioengineered telomerase-specific oncolytic adenovirus, OBP-301, efficiently kills $CD133^+$ cancer stem–like cells that have elevated telomerase activity through enhanced E1A-mediated cell-cycle mobilization and S-phase trapping. By using FUCCI technology in combination with tumor sphere culture, we visualized virus penetration, cell-cycle dynamics, and the subsequent elimination of quiescent cancer stem–like cells in dormant tumor spheres (Supplementary Fig. S15A).

Cancer stem–like cells have been shown to be highly resistant to chemotherapeutic agents (32, 33) and ionizing radiation (24–26). As expected, $CD133^+$ human gastric cancer cells were more resistant to conventional therapies than $CD133^-$ cells; OBP-301, however, efficiently reduced the viability of $CD133^+$ cells, similar to their reduction of viability of $CD133^-$ cells. Moreover, we showed that OBP-301 significantly reduced the stem cell properties of $CD133^+$ cells *in vitro* and *in vivo* compared with conventional chemoradiotherapy and further sensitized $CD133^+$ cancer stem–like cells to chemotherapy. These findings indicate that OBP-301 is a promising anticancer therapy to eliminate cancer stem–like cells more efficiently than conventional therapy in the clinical setting.

Recent studies have showed that p53 and $p21^{cip1/waf1}$ maintain the quiescent state in hematopoietic stem cells (34, 35). Moreover, $p27^{kip1}$ has been suggested to be involved in suppression of the transition from the G_0 phase to G_1–S phases (36, 37). Cancer stem–like cells maintain a more quiescent state than non–cancer stem–like cells, which is associated with cancer stem–like cell resistance to conventional therapies (9, 10). OBP-301 induced S and G_2–M phase entry and subsequent cell death in quiescent $CD133^+$ cells through upregulation of E2F1-related proteins and downregulation of p53-related and p27 proteins in an E1A-dependent manner. A recent report suggested that suppression of the p53-mediated G_1 checkpoint is required for E2F1-induced S-phase entry (38). Furthermore, adenoviral E1A has been shown to suppress p53-mediated cell-cycle arrest after DNA damage (39). Thus, OBP-301 can inhibit cancer stem–like cells from maintaining a quiescent state and force them into cycling by not only upregulating E2F-related proteins but also downregulating p53-related and p27 proteins (Supplementary Fig. S15B), leading to the sensitization to chemotherapy.

FUCCI (23) is a powerful tool to visualize the quiescent state in cancer stem–like cells and the treatment dynamics of OBP-301. When tumor spheres were formed, $CD133^+$ cells maintained a quiescent state, which was defined by red fluorescent nuclei expressed in G_0 –G_1 phases. In contrast, S and G_2–M phase entry induced by OBP-301 could be clearly visualized as yellow and green fluorescent nuclei, respectively. Our data indicate that 3-dimensional cultures are extremely important for the maintenance of the quiescence of $CD133^+$ cells. FUCCI-based real-time imaging of the cell cycle provides a platform for the screening of candidate therapeutic agents that modulate the quiescent state of drug-resistant cancer stem–like cells.

In conclusion, we have clearly shown that a genetically-engineered oncolytic adenovirus, OBP-301, efficiently eradicates quiescent cancer stem–like cells in solid tumors by cell-cycle mobilization and S/G_2/M phase trapping. A phase I clinical trial of intratumoral injection of OBP-301 in patients with advanced solid tumors was recently completed and OBP-301 monotherapy was well tolerated by these patients (20). However, the difficulty of adenoviral delivery to inaccessible primary and metastatic tumor tissues is a major obstacle for clinical translation of this treatment modality. In this study, the combination therapy of OBP-301 with chemotherapy was highly effective antitumor therapy to eliminate both cancer stem–like and non–cancer stem–like cells in a xenograft model. Future clinical trials of intratumoral injection of OBP-301 in combination with conventional antitumor therapy are suggested by the results of the present study.

Disclosure of Potential Conflicts of Interest

Y. Urata is President & CEO of Oncolys BioPharma, Inc., the manufacturer of OBP-301 (Telomelysin). H. Tazawa and T. Fujiwara are consultants of Oncolys BioPharma, Inc. No potential conflicts of interest were disclosed by the other authors.

Authors' Contributions

Conception and design: S. Yano, H. Tazawa, R. M. Hoffman, T. Fujiwara
Development of methodology: S. Yano, H. Tazawa, Y. Hashimoto, S. Kuroda, H. Kishimoto
Acquisition of data (provided animals, provided facilities, etc): S. Yano, H. Tazawa, Y. Hashimoto
Analysis and interpretation of data (e.g., statistical analysis, biostatistics, computational analysis): S. Yano, H. Tazawa, Y. Hashimoto, Nagasaka, S. Kagawa, T. Fujiwara
Writing, review, and/or revision of manuscript: S. Yano, H. Tazawa, R. M. Hoffman, T. Fujiwara
Administrative, technical, or material support: Y. Urata, R. M. Hoffman
Study supervision: H. Tazawa, Y. Shirakawa, M. Nishizaki, T. Nagasaka, S. Kagawa, R. M. Hoffman, T. Fujiwara

Acknowledgments

The authors thank Yukinari Isomoto and Tomoko Sueishi for their technical support.

Published OnlineFirst September 30, 2013; DOI: 10.1158/1078-0432.CCR-13-0742

Grant Support

This work was supported, in part, by grants from the Ministry of Education, Culture, Sports, Science, and Technology of Japan (to T. Fujiwara, No. 22390256) and by grants from the Ministry of Health, Labour, and Welfare of Japan (to T. Fujiwara, No. 10103827, No. 09156285).

The costs of publication of this article were defrayed in part by the payment of page charges. This article must therefore be hereby marked *advertisement* in accordance with 18 U.S.C. Section 1734 solely to indicate this fact.

Received March 20, 2013; revised September 10, 2013; accepted September 10, 2013; published OnlineFirst September 30, 2013.

References

1. Goss PE, Chambers AF. Does tumour dormancy offer a therapeutic target? Nat Rev Cancer 2010;10:871–7.
2. Aguirre-Ghiso JA. Models, mechanisms and clinical evidence for cancer dormancy. Nat Rev Cancer 2007;7:834–46.
3. Reya T, Morrison SJ, Clarke MF, Weissman IL. Stem cells, cancer, and cancer stem cells. Nature 2001;414:105–11.
4. Pardal R, Clarke MF, Morrison SJ. Applying the principles of stem-cell biology to cancer. Nat Rev Cancer 2003;3:895–902.
5. Clarke MF, Dick JE, Dirks PB, Eaves CJ, Jamieson CH, Jones DL, et al. Cancer stem cells–perspectives on current status and future directions: AACR Workshop on cancer stem cells. Cancer Res 2006;66:9339–44.
6. Visvader JE, Lindeman GJ. Cancer stem cells in solid tumours: accumulating evidence and unresolved questions. Nat Rev Cancer 2008;8:755–68.
7. Trumpp A, Wiestler OD. Mechanisms of Disease: cancer stem cells–targeting the evil twin. Nat Clin Pract Oncol 2008;5:337–47.
8. Zhou BB, Zhang H, Damelin M, Geles KG, Grindley JC, Dirks PB. Tumour-initiating cells: challenges and opportunities for anticancer drug discovery. Nat Rev Drug Discov 2009;8:806–23.
9. Ito K, Bernardi R, Morotti A, Matsuoka S, Saglio G, Ikeda Y, et al. PML targeting eradicates quiescent leukaemia-initiating cells. Nature 2008;453:1072–8.
10. Saito Y, Uchida N, Tanaka S, Suzuki N, Tomizawa-Murasawa M, Sone A, et al. Induction of cell cycle entry eliminates human leukemia stem cells in a mouse model of AML. Nat Biotechnol 2010;28:275–80.
11. Alemany R, Balague C, Curiel DT. Replicative adenoviruses for cancer therapy. Nat Biotechnol 2000;18:723–7.
12. Russell SJ, Peng KW, Bell JC. Oncolytic virotherapy. Nat Biotechnol 2012;30:658–70.
13. Stracker TH, Carson CT, Weitzman MD. Adenovirus oncoproteins inactivate the Mre11-Rad50-NBS1 DNA repair complex. Nature 2002;418:348–52.
14. Flinterman M, Gaken J, Farzaneh F, Tavassoli M. E1A-mediated suppression of EGFR expression and induction of apoptosis in head and neck squamous carcinoma cell lines. Oncogene 2003;22:1965–77.
15. Yu D, Wolf JK, Scanlon M, Price JE, Hung MC. Enhanced c-erbB-2/neu expression in human ovarian cancer cells correlates with more severe malignancy that can be suppressed by E1A. Cancer Res 1993;53:891–8.
16. Eriksson M, Guse K, Bauerschmitz G, Virkkunen P, Tarkkanen M, Tanner M, et al. Oncolytic adenoviruses kill breast cancer initiating CD44+CD24-/low cells. Mol Ther 2007;15:2088–93.
17. Zhang X, Komaki R, Wang L, Fang B, Chang JY. Treatment of radioresistant stem-like esophageal cancer cells by an apoptotic gene-armed, telomerase-specific oncolytic adenovirus. Clin Cancer Res 2008;14:2813–23.
18. Kanai R, Rabkin SD, Yip S, Sgubin D, Zaupa CM, Hirose Y, et al. Oncolytic virus-mediated manipulation of DNA damage responses: synergy with chemotherapy in killing glioblastoma stem cells. J Natl Cancer Inst 2012;104:42–55.
19. Kawashima T, Kagawa S, Kobayashi N, Shirakiya Y, Umeoka T, Teraishi F, et al. Telomerase-specific replication-selective virotherapy for human cancer. Clin Cancer Res 2004;10:285–92.
20. Nemunaitis J, Tong AW, Nemunaitis M, Senzer N, Phadke AP, Bedell C, et al. A phase I study of telomerase-specific replication competent oncolytic adenovirus (telomelysin) for various solid tumors. Mol Ther 2010;18:429–34.
21. Yokozaki H. Molecular characteristics of eight gastric cancer cell lines established in Japan. Pathol Int 2000;50:767–77.
22. Hashimoto Y, Watanabe Y, Shirakiya Y, Uno F, Kagawa S, Kawamura H, et al. Establishment of biological and pharmacokinetic assays of telomerase-specific replication-selective adenovirus. Cancer Sci 2008;99:385–90.
23. Sakaue-Sawano A, Kurokawa H, Morimura T, Hanyu A, Hama H, Osawa H, et al. Visualizing spatiotemporal dynamics of multicellular cell-cycle progression. Cell 2008;132:487–98.
24. Baumann M, Krause M, Hill R. Exploring the role of cancer stem cells in radioresistance. Nat Rev Cancer 2008;8:545–54.
25. Bao S, Wu Q, McLendon RE, Hao Y, Shi Q, Hjelmeland AB, et al. Glioma stem cells promote radioresistance by preferential activation of the DNA damage response. Nature 2006;444:756–60.
26. Phillips TM, McBride WH, Pajonk F. The response of CD24(−/low)/CD44 +breast cancer-initiating cells to radiation. J Natl Cancer Inst 2006;98:1777–85.
27. Nakayama KI, Nakayama K. Ubiquitin ligases: cell-cycle control and cancer. Nat Rev Cancer 2006;6:369–81.
28. Lee J, Kotliarova S, Kotliarov Y, Li A, Su Q, Donin NM, et al. Tumor stem cells derived from glioblastomas cultured in bFGF and EGF more closely mirror the phenotype and genotype of primary tumors than do serum-cultured cell lines. Cancer Cell 2006;9:391–403.
29. Ricci-Vitiani L, Lombardi DG, Pilozzi E, Biffoni M, Todaro M, Peschle C, et al. Identification and expansion of human colon-cancer-initiating cells. Nature 2007;445:111–5.
30. Fujiwara T, Kagawa S, Kishimoto H, Endo Y, Hioki M, Ikeda Y, et al. Enhanced antitumor efficacy of telomerase-selective oncolytic adenoviral agent OBP-401 with docetaxel: preclinical evaluation of chemovirotherapy. Int J Cancer 2006;119:432–40.
31. Liu D, Kojima T, Ouchi M, Kuroda S, Watanabe Y, Hashimoto Y, et al. Preclinical evaluation of synergistic effect of telomerase-specific oncolytic virotherapy and gemcitabine for human lung cancer. Mol Cancer Ther 2009;8:980–7.
32. Dean M, Fojo T, Bates S. Tumour stem cells and drug resistance. Nat Rev Cancer 2005;5:275–84.
33. Ma S, Lee TK, Zheng BJ, Chan KW, Guan XY. CD133+ HCC cancer stem cells confer chemoresistance by preferential expression of the Akt/PKB survival pathway. Oncogene 2008;27:1749–58.
34. Cheng T, Rodrigues N, Shen H, Yang Y, Dombkowski D, Sykes M, et al. Hematopoietic stem cell quiescence maintained by p21cip1/waf1. Science 2000;287:1804–8.
35. Liu Y, Elf SE, Miyata Y, Sashida G, Huang G, Di Giandomenico S, et al. p53 regulates hematopoietic stem cell quiescence. Cell Stem Cell 2009;4:37–48.
36. Sutterluty H, Chatelain E, Marti A, Wirbelauer C, Senften M, Muller U, et al. p45SKP2 promotes p27Kip1 degradation and induces S phase in quiescent cells. Nat Cell Biol 1999;1:207–14.
37. Kamura T, Hara T, Matsumoto M, Ishida N, Okumura F, Hatakeyama S, et al. Cytoplasmic ubiquitin ligase KPC regulates proteolysis of p27 (Kip1) at G1 phase. Nat Cell Biol 2004;6:1229–35.
38. Lomazzi M, Moroni MC, Jensen MR, Frittoli E, Helin K. Suppression of the p53- or pRB-mediated G1 checkpoint is required for E2F-induced S-phase entry. Nat Genet 2002;31:190–4.
39. Steegenga WT, van Laar T, Riteco N, Mandarino A, Shvarts A, van der Eb AJ, et al. Adenovirus E1A proteins inhibit activation of transcription by p53. Mol Cell Biol 1996;16:2101–9.

Molecular Cancer Therapeutics

Dual Programmed Cell Death Pathways Induced by p53 Transactivation Overcome Resistance to Oncolytic Adenovirus in Human Osteosarcoma Cells

Joe Hasei[1], Tsuyoshi Sasaki[1], Hiroshi Tazawa[2,4], Shuhei Osaki[1], Yasuaki Yamakawa[1], Toshiyuki Kunisada[1,3], Aki Yoshida[1], Yuuri Hashimoto[2], Teppei Onishi[2], Futoshi Uno[2], Shunsuke Kagawa[2], Yasuo Urata[5], Toshifumi Ozaki[1], and Toshiyoshi Fujiwara[2]

Abstract

Tumor suppressor p53 is a multifunctional transcription factor that regulates diverse cell fates, including apoptosis and autophagy in tumor biology. p53 overexpression enhances the antitumor activity of oncolytic adenoviruses; however, the molecular mechanism of this occurrence remains unclear. We previously developed a tumor-specific replication-competent oncolytic adenovirus, OBP-301, that kills human osteosarcoma cells, but some human osteosarcoma cells were OBP-301–resistant. In this study, we investigated the antitumor activity of a p53-expressing oncolytic adenovirus, OBP-702, and the molecular mechanism of the p53-mediated cell death pathway in OBP-301–resistant human osteosarcoma cells. The cytopathic activity of OBP-702 was examined in OBP-301–sensitive (U2OS and HOS) and OBP-301–resistant (SaOS-2 and MNNG/HOS) human osteosarcoma cells. The molecular mechanism in the OBP-702–mediated induction of two cell death pathways, apoptosis and autophagy, was investigated in OBP-301–resistant osteosarcoma cells. The antitumor effect of OBP-702 was further assessed using an orthotopic OBP-301–resistant MNNG/HOS osteosarcoma xenograft tumor model. OBP-702 suppressed the viability of OBP-301–sensitive and -resistant osteosarcoma cells more efficiently than OBP-301 or a replication-deficient p53-expressing adenovirus (Ad-p53). OBP-702 induced more profound apoptosis and autophagy when compared with OBP-301 or Ad-p53. E1A-mediated *miR-93/106b* upregulation induced p21 suppression, leading to p53-mediated apoptosis and autophagy in OBP-702–infected cells. p53 overexpression enhanced adenovirus-mediated autophagy through activation of damage-regulated autophagy modulator (DRAM). Moreover, OBP-702 suppressed tumor growth in an orthotopic OBP-301–resistant MNNG/HOS xenograft tumor model. These results suggest that OBP-702–mediated p53 transactivation is a promising antitumor strategy to induce dual apoptotic and autophagic cell death pathways via regulation of miRNA and DRAM in human osteosarcoma cells. *Mol Cancer Ther; 12(3); 314–25. ©2012 AACR.*

Introduction

Osteosarcoma is one of the most common malignant tumors in young children (1, 2). Current treatment strategies, which consist of multi-agent chemotherapy and aggressive surgery, have significantly improved the cure rate and prognosis of patients with osteosarcoma. In fact, over the past 30 years, the 5-year survival rate has increased from 10% to 70% (3–5). Even in patients with osteosarcoma with metastases at diagnosis, the 5-year survival rate has reached 20% to 30% in response to chemotherapy and surgical removal of primary and metastatic tumors (6). However, treatment outcomes for patients with osteosarcomas have further improved over the last few years. Therefore, the development of novel therapeutic strategies is required to improve the clinical outcomes in patients with osteosarcomas.

Tumor-specific replication-competent oncolytic viruses are being developed as novel anticancer therapy, in which the promoters of cancer-related genes are used to regulate virus replication in a tumor-dependent manner. More than 85% of all human cancers express high telomerase activity to maintain the length of the telomeres during cell division, whereas normal somatic cells seldom show this enhanced telomerase activity (7, 8). Telomerase activity has also been detected in 44% to 81% of bone and

Authors' Affiliations: Departments of [1]Orthopaedic Surgery, [2]Gastroenterological Surgery, and [3]Medical Materials for Musculoskeletal Reconstruction, Okayama University Graduate School of Medicine, Dentistry and Pharmaceutical Sciences; [4]Center for Innovative Clinical Medicine, Okayama University Hospital, Okayama; and [5]Oncolys BioPharma, Inc., Tokyo, Japan

Note: Supplementary data for this article are available at Molecular Cancer Therapeutics Online (http://mct.aacrjournals.org/).

Corresponding Author: Toshiyoshi Fujiwara, Department of Gastroenterological Surgery, Okayama University Graduate School of Medicine, Dentistry and Pharmaceutical Sciences, 2-5-1 Shikata-cho, Kita-ku, Okayama 700-8558, Japan. Phone: 81-86-235-7257; Fax: 81-86-221-8775; E-mail: toshi_f@md.okayama-u.ac.jp

doi: 10.1158/1535-7163.MCT-12-0869

soft-tissue sarcomas (9, 10). Telomerase activation is closely correlated with the expression of the human telomerase reverse transcriptase (*hTERT*) gene (11). On the basis of these data, we previously developed a telomerase-specific replication-competent oncolytic adenovirus OBP-301 (Telomelysin) in which the *hTERT* gene promoter drives the expression of the *E1A* and *E1B* genes (12). A phase I clinical trial of OBP-301, which was conducted in the United States on patients with advanced solid tumors, indicated that OBP-301 was well tolerated by patients (13). Recently, we reported that OBP-301 efficiently killed human bone and soft-tissue sarcoma cells (14, 15). However, some osteosarcoma cell lines were not sensitive to the antitumor effect of OBP-301. Therefore, to efficiently eliminate tumor cells with OBP-301, its antitumor effects need to be enhanced.

Cancer gene therapy is defined as the treatment of malignant tumors via the introduction of a therapeutic tumor suppressor gene or the abrogation of an oncogene. The tumor suppressor *p53* gene has an attractive tumor suppressor profile as a potent therapeutic transgene for induction of cell-cycle arrest, senescence, apoptosis, and autophagy (16). Dual cell death pathways, such as apoptosis and autophagy, induced by p53 transactivation are mainly involved in the suppression of tumor initiation and progression. However, among the p53 downstream target genes, p21, which is most rapidly and strongly induced during the DNA damage response, mainly induces cell-cycle arrest through suppression of apoptotic and autophagic cell death pathways (17, 18). Thus, p21 suppression may be a more effective strategy for the induction of apoptotic and autophagic cell death pathways in tumor cells, particularly when the tumor suppressor *p53* gene is overexpressed in tumor cells in response to cancer gene therapy.

A p53-expressing replication-deficient adenovirus (Ad-p53, Advexin) has previously been reported to induce an antitumor effect in the *in vitro* and *in vivo* settings (19, 20) as well as in some clinical studies (21–24). We recently reported that combination therapy with OBP-301 and Ad-p53 resulted in a more profound antitumor effect than monotherapy with either OBP-301 or Ad-p53 (25). Moreover, we generated armed OBP-301 expressing the wild-type *p53* tumor suppressor gene (OBP-702) and showed that OBP-702 suppressed the viability of various types of epithelial malignant cells more efficiently than did OBP-301 (26). OBP-702 induced a more profound apoptotic cell death effect than Ad-p53, likely via adenoviral E1A-mediated suppression of anti-apoptotic p21 in human epithelial malignant cells. However, it remained unclear whether OBP-702 efficiently induces an antitumor effect in human nonepithelial malignant cells, including osteosarcomas.

In the present study, we investigated the *in vitro* cytopathic efficacy of the p53-expressing telomerase-specific replication-competent oncolytic adenovirus, OBP-702, in human osteosarcoma cells, and we compared the induction level of apoptotic and autophagic cell deaths in OBP-301–resistant human osteosarcoma cells infected with OBP-301, OBP-702, and Ad-p53. The molecular mechanism by which OBP-702 mediates induction of apoptosis and autophagy was also investigated. Finally, the *in vivo* antitumor effect of OBP-702 was evaluated using an orthotopic OBP-301–resistant human osteosarcoma xenograft tumor model.

Materials and Methods

Cell lines

The human osteosarcoma cell lines, HOS and SaOS-2, were kindly provided by Dr. Satoru Kyo (Kanazawa University, Ishikawa, Japan). These cells were propagated as monolayer cultures in Dulbecco's Modified Eagle's Medium. The human osteosarcoma cell line, U2OS, was obtained from the American Type Culture Collection and was grown in McCoy's 5a Medium. The human osteosarcoma cell line, MNNG/HOS, was purchased from DS Pharma Biomedical and was maintained in Eagle's Minimum Essential Medium containing 1% nonessential amino acids. All media were supplemented with 10% FBS, 100 U/mL penicillin, and 100 mg/mL streptomycin. The normal human lung fibroblast (NHLF) cell line, NHLF, was obtained from TaKaRa Biomedicals. NHLF cells were propagated as monolayer culture in the medium recommended by the manufacturer. Although cell lines were not authenticated by the authors, cells were immediately expanded after receipt and stored in liquid N_2. Cells were not cultured for more than 5 months following resuscitation. The cells were maintained at 37°C in a humidified atmosphere with 5% CO_2.

Recombinant adenoviruses

The recombinant telomerase-specific replication-competent adenovirus OBP-301 (Telomelysin), in which the promoter element of the *hTERT* gene drives the expression of *E1A* and *E1B* genes, was previously constructed and characterized (12, 27). For OBP-301–mediated induction of exogenous *p53* gene expression, we recently generated OBP-702, in which a human wild-type *p53* gene expression cassette was inserted into the *E3* region (Supplementary Fig. S1; ref. 26). Ad-p53 is a replication-defective adenovirus serotype 5 vector with a *p53* gene expression cassette at the *E1* region (19, 20). Recombinant viruses were purified by ultracentrifugation using cesium chloride step gradients, their titers were determined by a plaque-forming assay using 293 cells and they were stored at −80°C.

Cell viability assay

Cells were seeded on 96-well plates at a density of 1×10^3 cells/well 24 hours before viral infection. All cell lines were infected with OBP-702 at multiplicity of infections (MOI) of 0, 0.1, 1, 10, 50, or 100 plaque-forming units (PFU)/cell. Cell viability was determined on days 1, 2, 3, and 5 after virus infection using Cell Proliferation Kit II (Roche Molecular Biochemicals). The 50% inhibiting dose (ID_{50}) value of OBP-702 for each cell line was calculated

using cell viability data obtained on day 5 after virus infection.

Time-lapse confocal laser microscopy

GFP-expressing MNNG/HOS (MNNG/HOS-GFP) cells were established by stable transfection with GFP expression plasmid using Lipofectamine LTX (Invitrogen). MNNG/HOS-GFP and NHLF cells were seeded in 35-mm glass-based dishes at a density of 1×10^5 cells/dish 24 hours before infection and were infected with OBP-702 at an MOI of 10 PFU/cell for 72 hours. Phase-contrast and fluorescence time-lapse recordings were obtained to concomitantly analyze cell morphology and GFP expression using an inverted FV10i confocal laser scanning microscopy (OLYMPUS).

Western blot analysis

SaOS-2 and MNNG/HOS cells, seeded in a 100-mm dish at a density of 1×10^5 cells/dish, were infected with OBP-301, OBP-702, or Ad-p53 at the indicated MOIs. In contrast, SaOS-2 cells were transfected with 10 nmol/L *miR-93* (Ambion), *miR-106b* (Ambion), or control miRNA (Ambion) 24 hours before Ad-p53 infection and infected with Ad-p53 at an MOI of 100 for 48 hours. Whole-cell lysates were prepared in a lysis buffer [50 mmol/L Tris-HCl (pH 7.4), 150 mmol/L NaCl, 1% Triton X-100] containing a protease inhibitor cocktail (Complete Mini; Roche) at the indicated time points. Proteins were electrophoresed on 6% to 15% SDS-PAGE and were transferred to polyvinylidene difluoride membranes (Hybond-P; GE Health Care). Blots were blocked with 5% non-fat dry milk in TBS-T (Tris-buffered saline and 0.1% Tween-20, pH 7.4). The primary antibodies used were: rabbit anti-PARP polyclonal antibody (pAb; Cell Signaling Technology), mouse anti-p53 monoclonal antibody (mAb; Calbiochem), mouse anti-$p21^{WAF1}$ mAb (Calbiochem), rabbit anti-E2F1 pAb (Santa Cruz Biotechnology), mouse anti-Ad5 E1A mAb (BD PharMingen), rabbit anti-microtubule-associated protein 1 light chain 3 (LC3) pAb [Medical & Biological Laboratories (MBL)], mouse anti-p62 mAb (MBL), rabbit anti-damage-regulated autophagy modulator (DRAM) pAb (Abgent), and mouse anti-β-actin mAb (Sigma-Aldrich).

Flow cytometric analysis

To analyze the active caspase-3 expression, cells were incubated for 20 minutes on ice in Cytofix/Cytoperm solution (BD Biosciences), labeled with phycoerythrin (PE)-conjugated rabbit anti-active caspase-3 mAb (BD Biosciences) for 30 minutes, and then analyzed using FACS array (BD Biosciences).

To evaluate the sub-G_1 population, which is a apoptosis indicator, in SaOS-2 cells after virus infection, SaOS-2 cells were seeded in a 100-mm dish at a density of 1×10^6 cells/dish 24 hours before viral infection and were infected with mock, OBP-301, Ad-p53, or OBP-702 at an MOI of 10 PFUs/cell for 48 hours. Cells were trypsinized and resuspended in original supernatant to ensure that both attached and nonattached cells were analyzed. Cells stained with propidium iodide were analyzed using FACS array (BD Biosciences).

Quantitative real-time reverse transcription PCR analysis

To evaluate the expressions of *miR-93* and *miR-106b* in tumor cells after OBP-702 infection, SaOS-2 and MNNG/HOS cells were seeded on 6-well plates at a density of 2×10^5 cells/well 24 hours before viral infection and were infected with OBP-702 at MOIs of 0, 1, 5, 10, 50, or 100 PFU/cell. Three days after virus infection, total RNA was extracted from the cells using a miRNeasy Mini Kit (Qiagen). The concentration and quality of RNA were assessed using a Nanodrop spectrophotometer. cDNA was synthesized from 10 ng of total RNA using the TaqMan MicroRNA Reverse Transcription Kit (Applied Biosystems), and quantitative real-time reverse transcription (RT)-PCR was carried out using the Applied Biosystems StepOnePlus real-time PCR System. The expressions of *miR-93* and *miR-106b* were defined from the threshold cycle (C_t), and relative expression levels were calculated using the $2^{-\Delta\Delta C_t}$ method after normalization with reference to the expression of U6 small nuclear RNA.

In vivo orthotopic MNNG/HOS xenograft tumor model

Animal experimental protocols were approved by the Ethics Review Committee for Animal Experimentation of Okayama University School of Medicine (Okayama, Japan). MNNG/HOS cells (5×10^6 cells per site) were inoculated into the tibias of female athymic nude mice aged 6 to 7 weeks (CLEA Japan). Palpable tumors developed within 21 days and were permitted to grow to approximately 5 to 6 mm in diameter. At that stage, a 50-μL volume of solution containing OBP-702, OBP-301, or Ad-p53 at a dose of 1×10^8 PFU or PBS was injected into the tumors for 3 cycles every 2 days. Tumor volume was monitored by computed tomographic (CT) imaging once a week after virus infection.

Three-dimensional computed tomography imaging

The tumor volume and formation of osteolytic lesions were evaluated using three-dimensional CT (3D-CT) imaging (ALOKA Latheta LCT-200; Hitachi Aloka Medical). The tumor volume was calculated by INTAGE Realia software (Cybernet Systems).

Histopathologic analysis

Tumors were fixed in 10% neutralized formalin and embedded in paraffin blocks. Sections were stained with hematoxylin/eosin and analyzed by light microscopy.

Statistical analysis

Data are expressed as means ± SD. Student *t* test was used to compare differences between groups. Statistical significance was defined as $P < 0.05$.

Results

In vitro cytopathic efficacy of OBP-702 against human osteosarcoma cell lines

To evaluate the *in vitro* cytopathic activity of OBP-702, we used the 2 OBP-301–sensitive human osteosarcoma cells (HOS and U2OS) and the 2 OBP-301–resistant human osteosarcoma cells (SaOS-2 and MNNG/HOS) that were recently described (14). The cell viability of each cell was assessed over 5 days after infection using the XTT assay. OBP-702 infection suppressed the viability of OBP-301–sensitive and -resistant cells in dose- and time-dependent manners (Fig. 1A and B). When the ID_{50} values of OBP-702 in all 4 human osteosarcoma cells were compared with those of OBP-301 calculated in a previous report (14), all cell lines were more sensitive to OBP-702 than to OBP-301 (Table 1). The ID_{50} values of OBP-702 were also lower than those of Ad-p53 (Supplementary Fig. S2). However, OBP-702 did not exhibit any cytopathic effect in NHLF cells (Fig. 1B). When GFP-expressing MNNG/HOS-GFP cells were cocultured with human normal NHLF cells, OBP-702 infection showed a cytopathic effect (confirmed by observation of round-shaped morphologic changes) in MNNG/HOS-GFP cells but not in NHLF cells (Fig. 1C). These results indicate that OBP-702 was more cytopathic than OBP-301 for human osteosarcoma cells but was not cytopathic for normal human cells.

Increased induction of apoptosis by OBP-702 when compared with OBP-301 or Ad-p53

We next investigated whether OBP-702 induces more profound apoptosis when compared with OBP-301 or Ad-p53. OBP-301–resistant SaOS-2 and MNNG/HOS cells

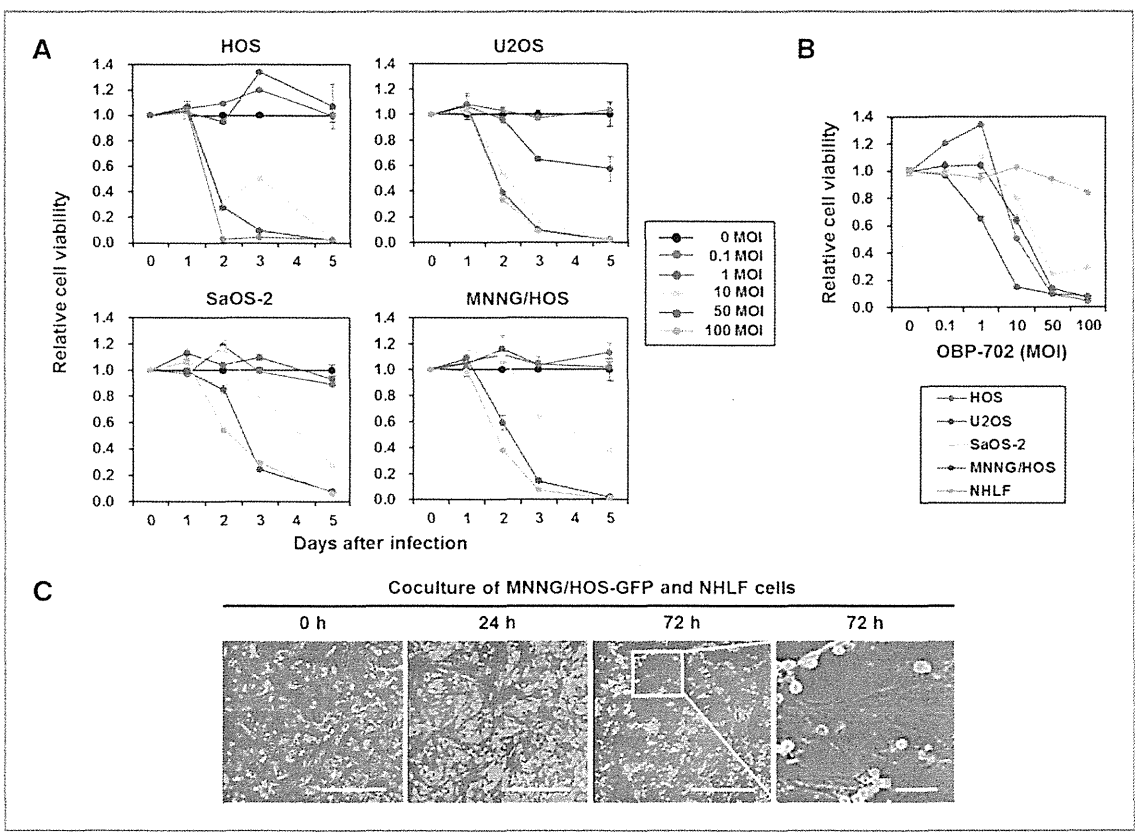

Figure 1. *In vitro* cytopathic effect of OBP-702 in human osteosarcoma cell lines. A, OBP-301–sensitive (HOS and U2OS) and OBP-301–resistant (SaOS-2 and MNNG/HOS) human osteosarcoma cells were infected with OBP-702 at the indicated MOI, and cell viability was quantified over 5 days using the XTT assay. Cell viability was calculated relative to that of the mock-infected group on each day, which was set at 1.0. Cell viability data are expressed as mean values ± SD ($n = 5$). B, four human osteosarcoma cells and one normal fibroblast NHLF cell were seeded 24 hours before viral infection and were infected with OBP-702 at the indicated MOIs, and cell viability was examined on day 5 using the XTT assay. Cell viability was calculated relative to that of the mock-infected group, which was set at 1.0. Cell viability data are expressed as mean ± SD ($n = 5$). C, time lapse images of cytopathic effect of OBP-702 in coculture of GFP-expressing MNNG/HOS cells with human normal fibroblast NHLF cells. MNNG/HOS-GFP cells coincubated with NHLF cells were recorded for 72 hours after OBP-702 infection at an MOI of 10. Three images on the left are low magnification and one image on the right is high magnification of the area outlined by a white square. Left scale bars, 100 μm. Right scale bar, 10 μm.

Table 1. Comparison of ID_{50} values of OBP-301 and OBP-702 in various human osteosarcoma cell lines

Cell lines	Sensitivity to OBP-301	Cell type	Relative hTERT mRNA expression	ID_{50} value[a] (MOI)		Ratio[b] (OBP-702/ OBP-301)
				OBP-301	OBP-702	
SaOS-2	Resistant	ALT	Negative	98.1	5.5	0.06
MNNG/HOS	Resistant	Non-ALT	1	97.3	6.7	0.07
U2OS	Sensitive	ALT	0.3	38.2	1.2	0.03
HOS	Sensitive	Non-ALT	4.3	43.0	4.5	0.10

[a]The ID_{50} values of OBP-702 and OBP-301 were calculated from the data of XTT assay on day 5 after infection.
[b]The ratio was calculated from the division of the ID_{50} value of OBP-702 by the ID_{50} value of OBP-301.

were infected with OBP-702, OBP-301, or Ad-p53, and apoptosis was assessed by Western blot and flow cytometric analyses. Western blot analysis showed that SaOS-2 cells exhibited the cleavage of PARP after infection with OBP-702 (>5 MOIs) or Ad-p53 (>50 MOIs), whereas MNNG/HOS cells had the cleavage of PARP after infection with OBP-702 (>5 MOIs) but not Ad-p53 (Fig. 2A). In contrast, OBP-301 did not induce apoptosis (data not shown). Furthermore, flow cytometric analysis showed that OBP-702 infection (10 MOIs) significantly increased the percentage of apoptotic cells with active caspase-3 when compared with Ad-p53 or OBP-301 at same doses in SaOS-2 and MNNG/HOS cells (Fig. 2B and C). Cell-cycle analysis also showed that OBP-702 (10 MOIs) induced the highest percentages of sub-G_1 population in SaOS-2 cells when compared with Ad-p53 or OBP-301 at same doses (Fig. 2D). These results suggest that OBP-702 induces increased apoptosis when compared with Ad-p53 or OBP-301 in human osteosarcoma cells.

p53 induction in human osteosarcoma cells infected with OBP-702

To investigate the molecular mechanism of OBP-702–induced apoptosis in human osteosarcoma cells, we evaluated p53 expression after OBP-702 infection in SaOS-2 (p53-null) and MNNG/HOS (p53-mutant) cells in which endogenous p53 expression level was confirmed by Western blot analysis (Supplementary Fig. S3). OBP-702 efficiently induced p53 expression in SaOS-2 and MNNG/HOS cells (Fig. 3A). The level of p53 expression was higher in OBP-702–treated cells than in Ad-p53–treated cells (Fig. 3A). Despite of OBP-702–induced high p53 expression, p53 downstream target p21 protein was induced only in Ad-p53–treated cells.

To investigate the effect of exogenous p53 overexpression in virus replication, we next compared the replication abilities of OBP-702 and OBP-301 in p53-null SaOS-2 cells by measuring the relative amounts of *E1A* copy numbers. The *E1A* copy number of OBP-702 was similar to that of OBP-301 in SaOS-2 cells (Supplementary Fig. S4). These results indicate that OBP-702 efficiently induces exogenous p53 expression without affecting p21 expression and virus replication in human osteosarcoma cells.

OBP-702–mediated upregulation of *miR-93* and *miR-106b* suppresses p21 expression

Adenoviral E1A protein has been shown to activate E2F1 expression (28), which is a multifunctional transcription factor that regulates diverse cell fates through induction of many target genes, including small noncoding miRNAs (29). Recently, E2F1-inducible *miR-93* and *miR-106b* have been shown to suppress p21 expression in human cancer cells (30). Therefore, we sought to investigate whether OBP-702 induces expressions of E2F1 and E2F1-regulated miRNAs (*miR-93* and *miR-106b*). OBP-702 infection activated E2F1 expression along with E1A accumulation in SaOS-2 and MNNG/HOS cells (Fig. 3B). The expression levels of *miR-93* and *miR-106b* were increased in association with E2F1 activation in OBP-702–infected SaOS-2 and MNNG/HOS cells (Fig. 3C). In contrast, E1A-deleted Ad-p53 infection did not increase expressions of E2F1 and E2F1-regulated *miR-93* and *miR-106b* (data not shown). Next, we assessed whether upregulation of *miR-93* and *miR-106b* efficiently suppresses p21 expression induced by Ad-p53–mediated p53 overexpression. Ad-p53 infection at MOIs of 10 and 100 efficiently induced p21 expression at 48 hours after infection in SaOS-2 cells (Supplementary Fig. S5). When SaOS-2 cells were infected with Ad-p53 at an MOI of 100 for 48 hours, pretransfection with *miR-93*, *miR-106b*, or both efficiently suppressed Ad-p53–induced p21 expression (Fig. 3D). Interestingly, both *miR-93*- and *miR-106b*–transfected SaOS-2 cells showed the 1.5-fold increased expression of cleaved PARP (C-PARP) in consistency with remarkable p21 downregulation when compared with those transfected with control miR. However, the expression level of C-PARP was not increased in the *miR-93*- or *miR-106b*–transfected SaOS-2 cells, although transfection with *miR-93* or *miR-106b* moderately decreased p21 expression. These results suggest that OBP-702 suppresses p21 expression through E1A-dependent upregulation of both E2F1-inducible *miR-93* and *miR-106b* and contributes to induction of apoptosis.

Increased induction of autophagy by OBP-702 when compared with OBP-301

Recently, we showed that oncolytic adenovirus OBP-301 mainly induces programmed cell death in association with autophagy rather than apoptosis in human tumor

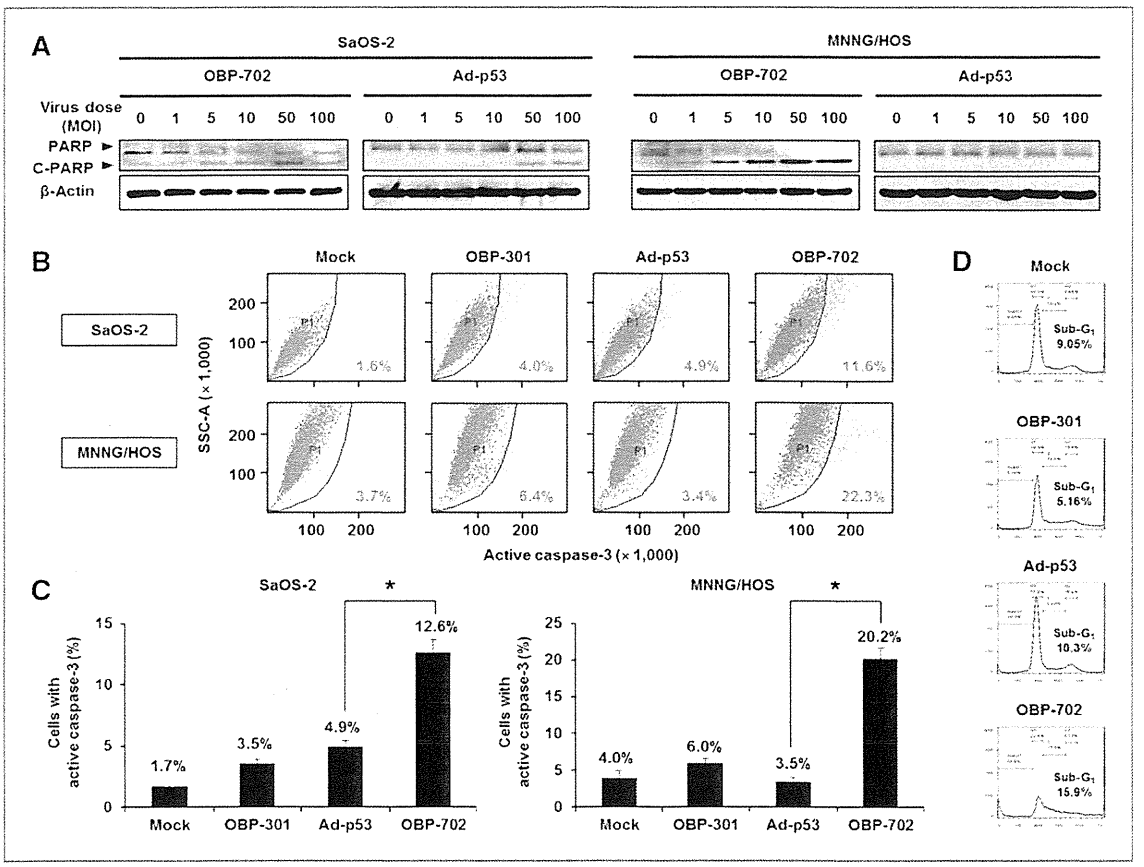

Figure 2. OBP-702 induces increased apoptosis when compared with OBP-301 or Ad-p53. A, OBP-301–resistant SaOS-2 and MNNG/HOS cells were infected with OBP-702 or Ad-p53 at the indicated MOIs for 72 hours. Cell lysates were subjected to Western blot analysis for the C-PARP and PARP. β-Actin was assayed as a loading control. B–D, SaOS-2 and MNNG/HOS cells were infected with OBP-702, OBP-301, or Ad-p53 at an MOI of 10 for 48 hours. Mock-infected cells were used as control. Caspase-3 activation was quantified using the flow cytometric analysis. Representative flow cytometric data are shown in B. The mean percentage of SaOS-2 cells and MNNG/HOS cells that express active caspase-3 was calculated on the basis of 3 independent experiments (C). The cell-cycle state was analyzed by flow cytometry in SaOS-2 cells after staining with propidium iodide. Representative cell-cycle data are shown (D). The percentage of sub-G_1 population was expressed in each graph. Bars, SD. Statistical significance was determined using Student *t* test. *, $P < 0.05$.

cells (31). Therefore, we next investigated whether OBP-702 induces more profound autophagy than does OBP-301. Western blot analysis revealed that OBP-702 infection showed increased autophagy, which was confirmed by conversion of LC3-I to LC3-II (increased ratio of LC3-II/LC3-I) and p62 downregulation, when compared with OBP-301 in MNNG/HOS cells (Fig. 4A). Moreover, the expression level of the p53-induced modulator of autophagy, DRAM (32), was decreased after OBP-301 infection, but its expression was maintained after OBP-702 infection (Fig. 4A). As p53-mediated p21 overexpression is known to inhibit both apoptosis and autophagy (17, 18), we further evaluated whether miR-mediated p21 suppression is involved in the enhancement of p53-mediated autophagy induction. Ad-p53–induced autophagy was enhanced by *miR-93*- and *miR-106b*–mediated p21 suppression (Fig. 4B). These results suggest that OBP-702 induces more profound autophagy than does OBP-301 and that this effect occurs via p53-mediated DRAM activation and miR-mediated p21 suppression.

Enhanced antitumor effect of OBP-702 in an orthotopic xenograft tumor model

Finally, to assess the *in vivo* antitumor effect of OBP-702, we used an orthotopic MNNG/HOS tumor xenograft model. OBP-702, OBP-301, Ad-p53, or PBS were intratumorally injected for 3 cycles every 2 days. OBP-702 administration significantly suppressed tumor growth when compared with OBP-301, Ad-p53, or PBS in an orthotopic MNNG/HOS tumor model (Fig. 5A and B). 3D-CT examination revealed that OBP-702–treated tumors had less bone destruction than did OBP-301- or Ad-p53–treated

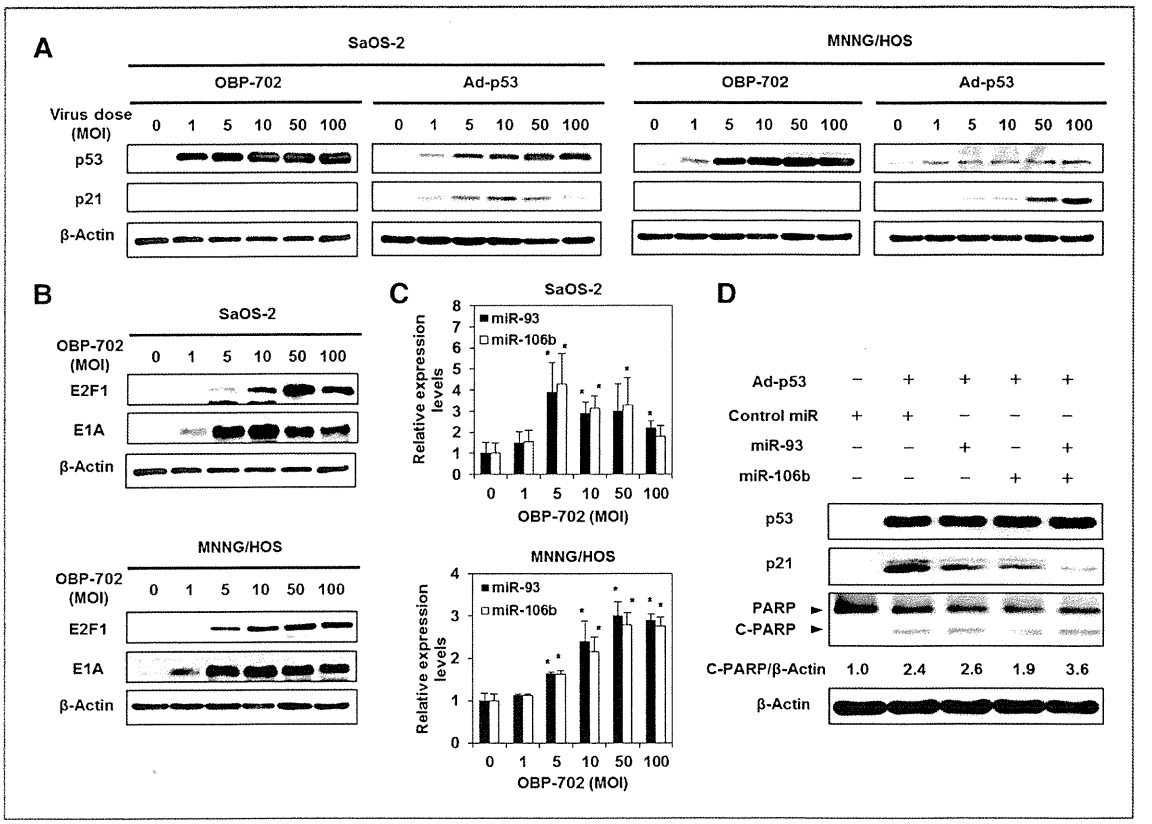

Figure 3. OBP-702 induces p53 overexpression with E1A-mediated p21 suppression via *miR-93* and *miR-106b* activation. A, expression of the p53 and p21 proteins in SaOS-2 and MNNG/HOS cells infected with OBP-702 or Ad-p53 at the indicated MOIs for 72 hours was assessed using Western blot analysis. B, expression of the E2F1 and viral E1A proteins in SaOS-2 and MNNG/HOS cells infected with OBP-702 at the indicated MOIs for 72 hours was assessed using Western blot analysis. C, expression of *miR-93* and *miR-106b* was assayed using qRT-PCR in SaOS-2 cells infected with OBP-702 at the indicated MOIs for 72 hours on 3 independent experiments. The values of *miR-93* and *miR-106b* at 0 MOI were set at 1, and the relative levels of *miR-93* and *miR-106b* at the indicated MOIs were plotted as fold induction. Bars, SD. Statistical significance was determined by Student *t* test. *, $P < 0.05$. D, SaOS-2 cells were transfected with 10 nmol/L *miR-93*, *miR-106*, or control miRNA 24 hours before Ad-p53 infection at an MOI of 100. At 48 hours after Ad-p53 infection, the expression levels of p53, p21, PARP, and C-PARP were examined by Western blot analysis. β-Actin was assayed as a loading control. By using ImageJ software, the expression level of C-PARP protein was calculated relative to its expression in the control miR–treated cells, whose expression level was designated as 1.0.

tumors (Fig. 5C). On histopathologic analysis, there were large necrotic areas in OBP-702–treated tumors but not in OBP-301- or Ad-p53–treated tumors (Fig. 5D). Moreover, the expression of the cell proliferation marker, Ki67, was also decreased, especially in OBP-702–treated tumor cells (Supplementary Fig. S6). These results suggest that OBP-702 eliminates tumor tissues more efficiently when compared with OBP-301 or Ad-p53.

Discussion

We previously reported that telomerase-specific replication-competent oncolytic adenovirus OBP-301 has strong antitumor activity in a variety of human epithelial and nonepithelial malignant cells (12, 14, 27). However, some human osteosarcoma cells were resistant to the cytopathic activity of OBP-301 (14). In this study, we showed that a novel p53-expressing oncolytic adenovirus, OBP-702, had increased *in vitro* and *in vivo* antitumor effects than did OBP-301 in human osteosarcoma cells (Fig. 1 and 5). OBP-702 induced increased apoptosis in association with p53 upregulation and p21 downregulation when compared with replication-deficient Ad-p53 (Fig. 2 and 3A). E1A-dependent upregulation of *miR-93* and *miR-106b* was involved in OBP-702–mediated suppression of p21 expression (Fig. 3). Moreover, p53-mediated DRAM activation with p21 suppression enhanced oncolytic adenovirus-mediated autophagy induction (Fig. 4). Recent studies suggest that transgene-expressing armed oncolytic adenoviruses are a promising antitumor strategy for induction of oncolytic and transgene-induced cell death (33). Although p53 overexpression has been shown to enhance antitumor

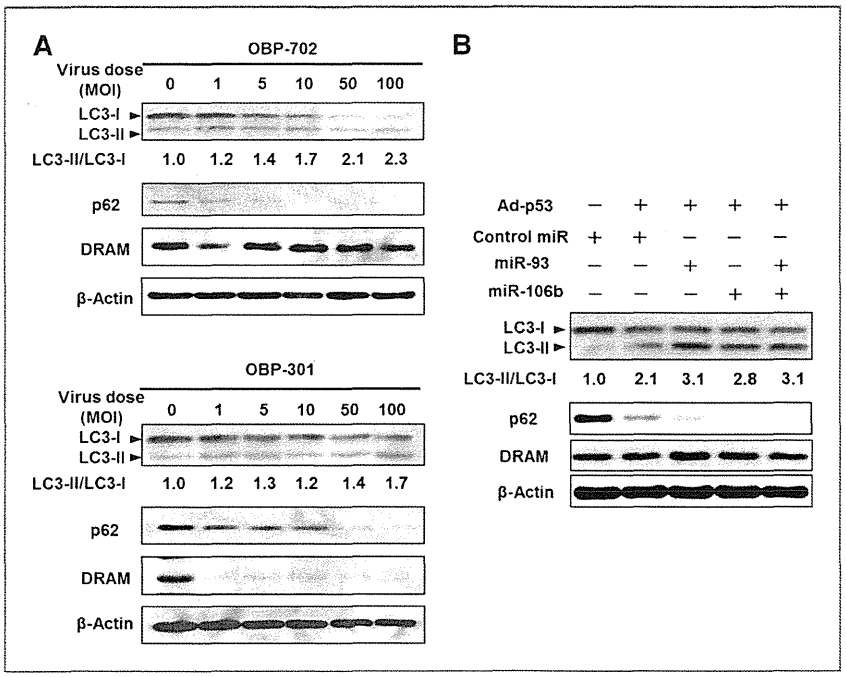

Figure 4. OBP-702 induces increased autophagy when compared with OBP-301. A, MNNG/HOS cells were infected with OBP-702 or OBP-301 at the indicated MOIs for 72 hours. Cell lysates were subjected to Western blot analysis for LC3, p62, and DRAM. B, SaOS-2 cells were transfected with 10 nmol/L *miR-93*, *miR-106*, or control miRNA 24 hours before Ad-p53 infection. At 48 hours after Ad-p53 infection at an MOI of 100, the expression levels of LC3, p62, and DRAM were examined by Western blot analysis. β-Actin was assayed as a loading control. By using ImageJ software, the ratio of LC3-II/LC3-I expressions was calculated relative to its expression in the mock-infected cells, whose expression level was designated as 1.0.

activity of oncolytic adenoviruses (34), the molecular mechanisms by which p53 mediates enhancement of the antitumor effect remain unclear. Recently, we reported that OBP-702 induces profound apoptosis through p53-dependent BAX upregulation and E1A-dependent p21 and MDM2 downregulation in epithelial malignant cells (26). Thus, oncolytic adenovirus-mediated p53 overexpression likely induces dual apoptotic and autophagic cell death pathways through p53-dependent BAX/DRAM activation and E1A-dependent p21/MDM2 suppression with E2F1-inducible *miR-93/106b* upregulation (Fig. 6).

OBP-702 efficiently suppressed the cell viability of both OBP-301–sensitive and -resistant osteosarcoma cells (Fig. 1). We previously reported that OBP-301–resistant SaOS-2 cells have no *hTERT* mRNA expression (Table 1), suggesting that SaOS-2 cells maintain telomere length through alternative lengthening of telomeres (ALT). As *hTERT* gene promoter is used for tumor-specific replication of OBP-301, ALT-type human osteosarcoma cells such as SaOS-2 cells may be resistant to OBP-301. However, ALT-type SaOS-2 cells showed similar sensitivity to OBP-702 as well as non–ALT-type MNNG/HOS cells (Fig. 1 and Table 1). These results suggest that p53 overexpression overcomes resistance to OBP-301 in ALT-type SaOS-2 cells. As the replication rate of OBP-702 was almost similar that of OBP-301 in ALT-type SaOS-2 cells (Supplementary Fig. S2), p53-induced cell death pathway would suppress the cell viability of ALT-type human osteosarcoma cells.

OBP-702–mediated p53 overexpression induced 2 types of programmed cell deaths (i.e., apoptosis and autophagy), thereby contributing to the enhancement of the antitumor effect of OBP-301 in human osteosarcoma cells (Fig. 2 and 4). As p53 downstream target p21 functions as a suppressor of apoptosis and autophagy (17, 18), p21 suppression may be a critical factor to induce dual programmed cell death pathways in response p53 overexpression. Suppression of p21 expression by genetic deletion or artificial p21 target microRNA has been shown to enhance the Ad-p53–induced apoptosis (18, 35). Inactivation of p21 by adenoviral E1A has been shown to enhance apoptosis in chemotherapeutic drug-treated human colon cancer cells that overexpress p53 (36). Genetic deletion of p21 has been also shown to induce autophagy in mouse embryonic fibroblasts treated with C (2)-ceramide or γ-irradiation (17). In contrast, p21 overexpression inhibited the Ad-p53–mediated apoptosis induction (18). Thus, E1A-mediated p21 downregulation would enhance p53-induced apoptosis and autophagy in OBP-702–infected cells.

E1A-dependent E2F1 activation and subsequent upregulation of E2F1-inducible miRNAs efficiently suppressed p21 expression, leading to the enhancement of p53-induced apoptosis and autophagy, in OBP-702–infected osteosarcoma cells (Figs. 2–4). Recent studies suggest that the cross-talk between p53 and E2F1 play a role in the regulation of diverse cell fates (37). For example, co-expression of p53 and E2F1 contributes to induction of apoptosis (38, 39). We previously showed

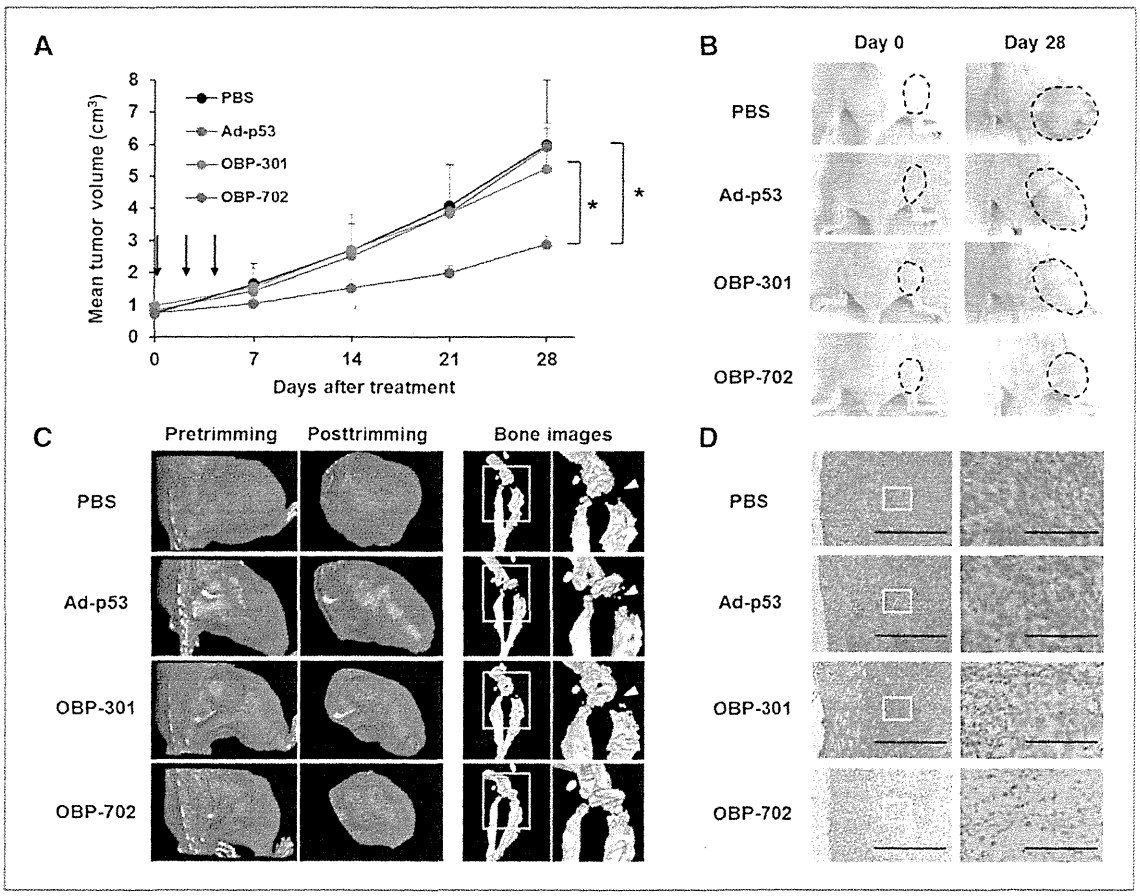

Figure 5. Antitumor effect of OBP-702 in an orthotopic MNNG/HOS osteosarcoma xenograft model. A, athymic nude mice were inoculated intratibially with MNNG/HOS cells (5×10^6 cells/site). Twenty-one days after inoculation (designated as day 0), Ad-p53, OBP-301, or OBP-702 were injected into the tumor with 1×10^8 PFUs on days 0, 2, and 4 (black arrows). PBS was used as a control. Three mice were used for each group. Each tumor volume was assessed by CT examination. Tumor growth was expressed as mean tumor volume ± SD. Statistical significance was determined by Student *t* test. *, $P < 0.05$. B, macroscopic appearance of MNNG/HOS tumors in nude mice on days 0 and 28 after treatment with PBS, Ad-p53, OBP-301, or OBP-702. Tumor masses are outlined by a dotted line. C, 3D-CT images of MNNG/HOS tumors. The tumor volumes were calculated by the image viewer (INTAGE Realia) based on 3D-CT images of tumors after trimming. The white arrowheads indicate the osteolytic areas within tumor tissues treated with PBS, Ad-p53, or OBP-301. Left side images are low magnification and right side images are high magnification of the area outlined by a white square. D, histologic analysis of the MNNG/HOS tumors. Tumor tissues were obtained on day 28 after first treatment with PBS, Ad-p53, OBP-301, or OBP-702. Paraffin-embedded sections of MNNG/HOS tumors were stained with hematoxylin and eosin solutions. There were large necrotic areas in MNNG/HOS tumors treated with OBP-702. Left side images are low magnification and right side images are high magnification of the area outlined by a white square. Left scale bars, 500 μm. Right scale bars, 100 μm.

that E2F1 enhanced Ad-p53–mediated apoptosis through p14ARF-dependent MDM2 downregulation (39) and that OBP-702 infection showed E1A-dependent MDM2 downregulation in association with apoptosis (26). Recently, E2F1 has been shown to suppress MDM2 expression by suppressing the promoter activity (40) or by inducing upregulation of *miR-25/32*, which targets MDM2 (41). Furthermore, E2F1-inducible *miR-93/106b* enhanced Ad-p53–induced apoptosis and autophagy via p21 suppression (Figs. 3D and 4B). Therefore, the cooperation between the MDM2/p53/p21 pathway and the E2F1/miRNA pathway may be involved in the induction of apoptotic and autophagic cell death in response to OBP-702.

OBP-702–mediated p53 overexpression enhanced autophagy that was induced by oncolytic adenovirus in human osteosarcoma cells. OBP-702 infection induced increased expression of DRAM and decreased expression of p62 when compared with OBP-301 (Fig. 4), suggesting that OBP-702–mediated p53 overexpression enhances autophagy through DRAM activation. We recently reported that OBP-301 induces autophagy through E1A-dependent activation of E2F1/*miR-7* pathway and subsequent suppression of EGF receptor

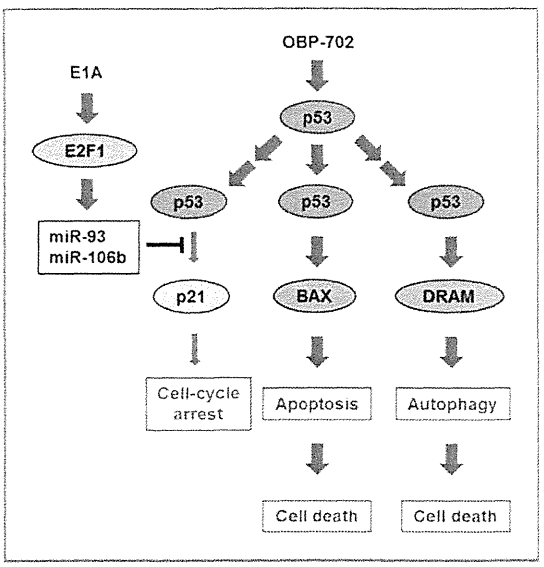

Figure 6. Outline of OBP-702–mediated induction of dual programmed cell death pathways. OBP-702 infection induces apoptosis and autophagy, leading to cell death, through p53-dependent BAX/DRAM upregulation and E1A-dependent p21 downregulation via E2F1-inducible *miR-93/106b* activation.

(EGFR; ref. 31). Restoration of p53 expression enhances the sensitivity to EGFR inhibitors in human cancer cells (42). Moreover, EGFR downregulation by transfection of specific antisense oligonucleotide promotes the differentiation status of human osteosarcoma U2OS cells (43). Thus, OBP-702 may induce differentiation as well as cell death through autophagy activation by DRAM upregulation and EGFR downregulation in human osteosarcoma cells.

The 3D-CT imaging system was a useful method to assess both tumor volume and bone destruction status in MNNG/HOS tumors. OBP-702–treated tumors were smaller and had less bone destruction than PBS-, Ad-p53-, or OBP-301–treated tumors (Fig. 5A and C). Recent reports have suggested that zoledronic acid suppresses tumor growth as well as osteolytic components in human osteosarcoma xenograft tumor models (44, 45). These results suggest that combination therapy with OBP-702 and zoledronic acid may be more effective and more protective against bone destruction in human osteosarcomas. Further study using a 3D-CT imaging system may provide important information about bone destruction status in osteosarcomas treated with OBP-702 and zoledronic acid.

Adenovirus-mediated *p53* gene therapy exerts an antitumor effect in human osteosarcoma cells (46). However, the antitumor activity of replication-deficient Ad-p53 is limited in some human osteosarcoma cells (47). Ad-p53–mediated p53 overexpression increases the sensitivity of human osteosarcoma cells to the chemotherapeutic drugs, cisplatin and doxorubicin (48). A synergistic antitumor effect between doxorubicin and roscovitine was also associated with autophagy induction in human osteosarcoma U2OS cells (49). As OBP-702 induced more profound apoptosis and autophagy than did OBP-301 or Ad-p53 (Fig. 2 and 4), combination therapy with OBP-702 and chemotherapeutic agents may be more effective than monotherapy with OBP-702. Moreover, a recent report has shown that p53-armed replication-competent oncolytic adenovirus is a safe antitumor agent in rodents and non-human primates (50). However, for clinical application of OBP-702, it must be necessary to establish the systemic delivery method and confirm the host biologic contributions in patients with cancer. Although there are some unsolved issues, the combination of p53-armed oncolytic adenovirus and chemotherapy may provide us a promising antitumor strategy against human osteosarcoma cells.

In conclusion, we clearly showed that the p53-expressing oncolytic adenovirus OBP-702 has a much stronger antitumor effect than does OBP-301. Oncolytic adenovirus-mediated *p53* gene transduction may induce dual apoptotic and autophagic cell death pathways through p53-dependent activation of cell death inducers and E1A-dependent suppression of cell death inhibitors, resulting in the enhancement of antitumor effect.

Disclosure of Potential Conflicts of Interest

Y. Urata is President & CEO of Oncolys BioPharma, Inc., the manufacturer of OBP-301 (Telomelysin). H. Tazawa and T. Fujiwara are consultants of Oncolys BioPharma, Inc. No potential conflicts of interest were disclosed by the other authors.

Authors' Contributions

Conception and design: J. Hasei, F. Uno, S. Kagawa, T. Ozaki, T. Fujiwara
Development of methodology: J. Hasei, F. Uno, S. Kagawa
Acquisition of data (provided animals, acquired and managed patients, provided facilities, etc.): J. Hasei, H. Tazawa, S. Osaki, Y. Yamakawa, A. Yoshida, T. Onishi, T. Ozaki
Analysis and interpretation of data (e.g., statistical analysis, biostatistics, computational analysis): J. Hasei, H. Tazawa, T. Fujiwara
Writing, review, and/or revision of the manuscript: J. Hasei, H. Tazawa, T. Kunisada, Y. Urata, T. Fujiwara
Administrative, technical, or material support (i.e., reporting or organizing data, constructing databases): H. Tazawa, T. Kunisada, Y. Hashimoto, S. Kagawa, Y. Urata, T. Ozaki
Study supervision: T. Sasaki, T. Kunisada, F. Uno, Y. Urata, T. Fujiwara

Acknowledgments

The authors thank Dr. Satoru Kyo (Kanazawa University) for providing the HOS and SaOS-2 cells and Tomoko Sueishi for her excellent technical support.

Grant Support

This study was supported by grants-in-aid from the Ministry of Education, Science, and Culture, Japan (T. Fujiwara) and grants from the Ministry of Health and Welfare, Japan (T. Fujiwara), and in part by the National Cancer Center Research and Development Fund (23-A-10) (T. Ozaki).

The costs of publication of this article were defrayed in part by the payment of page charges. This article must therefore be hereby marked *advertisement* in accordance with 18 U.S.C. Section 1734 solely to indicate this fact.

Received August 30, 2012; revised December 27, 2012; accepted December 29, 2012; published OnlineFirst January 11, 2013.

References

1. Ottaviani G, Jaffe N. The etiology of osteosarcoma. Cancer Treat Res 2009;152:15–32.
2. Damron TA, Ward WG, Stewart A. Osteosarcoma, chondrosarcoma, and Ewing's sarcoma: National Cancer Data Base Report. Clin Orthop Relat Res 2007;459:40–7.
3. Lewis IJ, Nooij MA, Whelan J, Sydes MR, Grimer R, Hogendoorn PC, et al. Improvement in histologic response but not survival in osteosarcoma patients treated with intensified chemotherapy: a randomized phase III trial of the European Osteosarcoma Intergroup. J Natl Cancer Inst 2007;99:112–28.
4. Bacci G, Longhi A, Versari M, Mercuri M, Briccoli A, Picci P. Prognostic factors for osteosarcoma of the extremity treated with neoadjuvant chemotherapy: 15-year experience in 789 patients treated at a single institution. Cancer 2006;106:1154–61.
5. Bielack SS, Kempf-Bielack B, Delling G, Exner GU, Flege S, Helmke K, et al. Prognostic factors in high-grade osteosarcoma of the extremities or trunk: an analysis of 1,702 patients treated on neoadjuvant cooperative osteosarcoma study group protocols. J Clin Oncol 2002; 20:776–90.
6. Siegel R, Naishadham D, Jemal A. Cancer statistics, 2012. CA Cancer J Clin 2012;62:10–29.
7. Buseman CM, Wright WE, Shay JW. Is telomerase a viable target in cancer? Mutat Res 2012;730:90–7.
8. Artandi SE, DePinho RA. Telomeres and telomerase in cancer. Carcinogenesis 2010;31:9–18.
9. Umehara N, Ozaki T, Sugihara S, Kunisada T, Morimoto Y, Kawai A, et al. Influence of telomerase activity on bone and soft tissue tumors. J Cancer Res Clin Oncol 2004;130:411–6.
10. Aogi K, Woodman A, Urquidi V, Mangham DC, Tarin D, Goodison S. Telomerase activity in soft-tissue and bone sarcomas. Clin Cancer Res 2000;6:4776–81.
11. Nakayama J, Tahara H, Tahara E, Saito M, Ito K, Nakamura H, et al. Telomerase activation by hTRT in human normal fibroblasts and hepatocellular carcinomas. Nat Genet 1998;18:65–8.
12. Kawashima T, Kagawa S, Kobayashi N, Shirakiya Y, Umeoka T, Teraishi F, et al. Telomerase-specific replication-selective virotherapy for human cancer. Clin Cancer Res 2004;10:285–92.
13. Nemunaitis J, Tong AW, Nemunaitis M, Senzer N, Phadke AP, Bedell C, et al. A phase I study of telomerase-specific replication competent oncolytic adenovirus (telomelysin) for various solid tumors. Mol Ther 2010;18:429–34.
14. Sasaki T, Tazawa H, Hasei J, Kunisada T, Yoshida A, Hashimoto Y, et al. Preclinical evaluation of telomerase-specific oncolytic virotherapy for human bone and soft tissue sarcomas. Clin Cancer Res 2011;17:1828–38.
15. Li G, Kawashima H, Ogose A, Ariizumi T, Xu Y, Hotta T, et al. Efficient virotherapy for osteosarcoma by telomerase-specific oncolytic adenovirus. J Cancer Res Clin Oncol 2011;137:1037–51.
16. Vousden KH, Prives C. Blinded by the light: the growing complexity of p53. Cell 2009;137:413–31.
17. Fujiwara K, Daido S, Yamamoto A, Kobayashi R, Yokoyama T, Aoki H, et al. Pivotal role of the cyclin-dependent kinase inhibitor p21WAF1/CIP1 in apoptosis and autophagy. J Biol Chem 2008;283:388–97.
18. Gorospe M, Cirielli C, Wang X, Seth P, Capogrossi MC, Holbrook NJ. p21(Waf1/Cip1) protects against p53-mediated apoptosis of human melanoma cells. Oncogene 1997;14:929–35.
19. Blagosklonny MV, el-Deiry WS. In vitro evaluation of a p53-expressing adenovirus as an anti-cancer drug. Int J Cancer 1996;67:386–92.
20. Zeng Y, Prabhu N, Meng R, Eldeiry W. Adenovirus-mediated p53 gene therapy in nasopharyngeal cancer. Int J Oncol 1997;11:221–6.
21. Clayman GL, el-Naggar AK, Lippman SM, Henderson YC, Frederick M, Merritt JA, et al. Adenovirus-mediated p53 gene transfer in patients with advanced recurrent head and neck squamous cell carcinoma. J Clin Oncol 1998;16:2221–32.
22. Swisher SG, Roth JA, Nemunaitis J, Lawrence DD, Kemp BL, Carrasco CH, et al. Adenovirus-mediated p53 gene transfer in advanced non-small-cell lung cancer. J Natl Cancer Inst 1999;91:763–71.
23. Shimada H, Matsubara H, Shiratori T, Shimizu T, Miyazaki S, Okazumi S, et al. Phase I/II adenoviral p53 gene therapy for chemoradiation resistant advanced esophageal squamous cell carcinoma. Cancer Sci 2006;97:554–61.
24. Fujiwara T, Tanaka N, Kanazawa S, Ohtani S, Saijo Y, Nukiwa T, et al. Multicenter phase I study of repeated intratumoral delivery of adenoviral p53 in patients with advanced non-small-cell lung cancer. J Clin Oncol 2006;24:1689–99.
25. Sakai R, Kagawa S, Yamasaki Y, Kojima T, Uno F, Hashimoto Y, et al. Preclinical evaluation of differentially targeting dual virotherapy for human solid cancer. Mol Cancer Ther 2010;9:1884–93.
26. Yamasaki Y, Tazawa H, Hashimoto Y, Kojima T, Kuroda S, Yano S, et al. A novel apoptotic mechanism of genetically engineered adenovirus-mediated tumour-specific p53 overexpression through E1A-dependent p21 and MDM2 suppression. Eur J Cancer 2012;48: 2282–91.
27. Hashimoto Y, Watanabe Y, Shirakiya Y, Uno F, Kagawa S, Kawamura H, et al. Establishment of biological and pharmacokinetic assays of telomerase-specific replication-selective adenovirus. Cancer Sci 2008;99:385–90.
28. Bagchi S, Raychaudhuri P, Nevins JR. Adenovirus E1A proteins can dissociate heteromeric complexes involving the E2F transcription factor: a novel mechanism for E1A trans-activation. Cell 1990;62: 659–69.
29. Emmrich S, Putzer BM. Checks and balances: E2F-microRNA crosstalk in cancer control. Cell Cycle 2010;9:2555–67.
30. Petrocca F, Vecchione A, Croce CM. Emerging role of miR-106b-25/miR-17-92 clusters in the control of transforming growth factor beta signaling. Cancer Res 2008;68:8191–4.
31. Tazawa H, Yano S, Yoshida R, Yamasaki Y, Sasaki T, Hashimoto Y, et al. Genetically engineered oncolytic adenovirus induces autophagic cell death through an E2F1-microRNA-7-epidermal growth factor receptor axis. Int J Cancer 2012;131:2939–50.
32. Crighton D, Wilkinson S, O'Prey J, Syed N, Smith P, Harrison PR, et al. DRAM, a p53-induced modulator of autophagy, is critical for apoptosis. Cell 2006;126:121–34.
33. Liu TC, Galanis E, Kirn D. Clinical trial results with oncolytic virotherapy: a century of promise, a decade of progress. Nat Clin Pract Oncol 2007;4:101–17.
34. van Beusechem VW, van den Doel PB, Grill J, Pinedo HM, Gerritsen WR. Conditionally replicative adenovirus expressing p53 exhibits enhanced oncolytic potency. Cancer Res 2002;62:6165–71.
35. Idogawa M, Sasaki Y, Suzuki H, Mita H, Imai K, Shinomura Y, et al. A single recombinant adenovirus expressing p53 and p21-targeting artificial microRNAs efficiently induces apoptosis in human cancer cells. Clin Cancer Res 2009;15:3725–32.
36. Chattopadhyay D, Ghosh MK, Mal A, Harter ML. Inactivation of p21 by E1A leads to the induction of apoptosis in DNA-damaged cells. J Virol 2001;75:9844–56.
37. Polager S, Ginsberg D. p53 and E2f: partners in life and death. Nat Rev Cancer 2009;9:738–48.
38. Wu X, Levine AJ. p53 and E2F-1 cooperate to mediate apoptosis. Proc Natl Acad Sci U S A 1994;91:3602–6.
39. Itoshima T, Fujiwara T, Waku T, Shao J, Kataoka M, Yarbrough WG, et al. Induction of apoptosis in human esophageal cancer cells by sequential transfer of the wild-type p53 and E2F-1 genes: involvement of p53 accumulation via ARF-mediated MDM2 down-regulation. Clin Cancer Res 2000;6:2851–9.
40. Tian X, Chen Y, Hu W, Wu M. E2F1 inhibits MDM2 expression in a p53-dependent manner. Cell Signal 2011;23:193–200.
41. Suh SS, Yoo JY, Nuovo GJ, Jeon YJ, Kim S, Lee TJ, et al. MicroRNAs/TP53 feedback circuitry in glioblastoma multiforme. Proc Natl Acad Sci U S A 2012;109:5316–21.
42. Huang S, Benavente S, Armstrong EA, Li C, Wheeler DL, Harari PM. p53 modulates acquired resistance to EGFR inhibitors and radiation. Cancer Res 2011;71:7071–9.
43. Salvatori L, Caporuscio F, Coroniti G, Starace G, Frati L, Russo MA, et al. Down-regulation of epidermal growth factor receptor induced by estrogens and phytoestrogens promotes the differentiation of U2OS human osteosarcoma cells. J Cell Physiol 2009;220: 35–44.

44. Dass CR, Choong PF. Zoledronic acid inhibits osteosarcoma growth in an orthotopic model. Mol Cancer Ther 2007;6:3263–70.
45. Labrinidis A, Hay S, Liapis V, Ponomarev V, Findlay DM, Evdokiou A. Zoledronic acid inhibits both the osteolytic and osteoblastic components of osteosarcoma lesions in a mouse model. Clin Cancer Res 2009;15:3451–61.
46. Ternovoi VV, Curiel DT, Smith BF, Siegal GP. Adenovirus-mediated p53 tumor suppressor gene therapy of osteosarcoma. Lab Invest 2006;86:748–66.
47. Hellwinkel OJ, Muller J, Pollmann A, Kabisch H. Osteosarcoma cell lines display variable individual reactions on wildtype p53 and Rb tumour-suppressor transgenes. J Gene Med 2005;7:407–19.
48. Ganjavi H, Gee M, Narendran A, Parkinson N, Krishnamoorthy M, Freedman MH, et al. Adenovirus-mediated p53 gene therapy in osteosarcoma cell lines: sensitization to cisplatin and doxorubicin. Cancer Gene Ther 2006;13:415–9.
49. Lambert LA, Qiao N, Hunt KK, Lambert DH, Mills GB, Meijer L, et al. Autophagy: a novel mechanism of synergistic cytotoxicity between doxorubicin and roscovitine in a sarcoma model. Cancer Res 2008;68:7966–74.
50. Su C, Cao H, Tan S, Huang Y, Jia X, Jiang L, et al. Toxicology profiles of a novel p53-armed replication-competent oncolytic adenovirus in rodents, felids, and nonhuman primates. Toxicol Sci 2008;106:242–50.

Gene Therapy (2013) **20,** 112–118

www.nature.com/gt

SHORT COMMUNICATION

A simple detection system for adenovirus receptor expression using a telomerase-specific replication-competent adenovirus

T Sasaki[1], H Tazawa[2,3], J Hasei[1], S Osaki [1], T Kunisada[1,4], A Yoshida[1], Y Hashimoto[3], S Yano[3], R Yoshida[3], S Kagawa[3], F Uno[3], Y Urata[5], T Ozaki[1] and T Fujiwara[3]

Adenovirus serotype 5 (Ad5) is frequently used as an effective vector for induction of therapeutic transgenes in cancer gene therapy or of tumor cell lysis in oncolytic virotherapy. Ad5 can infect target cells through binding with the coxsackie and adenovirus receptor (CAR). Thus, the infectious ability of Ad5-based vectors depends on the CAR expression level in target cells. There are conventional methods to evaluate the CAR expression level in human target cells, including flow cytometry, western blotting and immunohistochemistry. Here, we show a simple system for detection and assessment of functional CAR expression in human tumor cells, using the green fluorescent protein (GFP)-expressing telomerase-specific replication-competent adenovirus OBP-401. OBP-401 infection induced detectable GFP expression in CAR-expressing tumor cells, but not in CAR-negative tumor cells, nor in CAR-positive normal fibroblasts, 24 h after infection. OBP-401-mediated GFP expression was significantly associated with CAR expression in tumor cells. OBP-401 infection detected tumor cells with low CAR expression more efficiently than conventional methods. OBP-401 also distinguished CAR-positive tumor tissues from CAR-negative tumor and normal tissues in biopsy samples. These results suggest that GFP-expressing telomerase-specific replication-competent adenovirus is a very potent diagnostic tool for assessment of functional CAR expression in tumor cells for Ad5-based antitumor therapy.

Gene Therapy (2013) **20,** 112–118; doi:10.1038/gt.2011.213; published online 12 January 2012

Keywords: oncolytic virus; adenovirus; telomerase; sarcoma; GFP

INTRODUCTION

Adenovirus serotype 5 (Ad5) is widely and frequently used as an effective vector in cancer gene therapy and oncolytic virotherapy.[1–3] Adenovirus-mediated transgene transduction is a highly efficient method for induction of ectopic transgene expression in tumor cells.[1,2] The p53 tumor suppressor gene, which is a potential therapeutic transgene that may induce a very strong antitumor effect, has been transduced into tumor cells using a replication-deficient adenovirus vector (Ad-p53, Advexin, Intorgen Therapeutics, Inc., Austin, TX, USA), and Ad-p53 has been reported to induce an antitumor effect in clinical studies.[4–7] Recently, an Ad5-based replication-competent oncolytic adenovirus has been developed as a promising anticancer reagent for induction of tumor-specific cell lysis.[8,9] Ad5-based vectors infect human target cells through binding with the coxsackie and adenovirus receptor (CAR).[10] Thus, the infection efficiency of Ad5-based vectors mainly depends on the CAR expression level in tumor tissues.[11–17] Increased CAR expression has been frequently shown in tumor cells in various organs such as the brain,[18] thyroid,[19] esophagus,[20] gastrointestinal tract,[21] prostate,[14] bone and soft tissues.[22–24] However, tumor cells often show reduced CAR expression following tumor progression.[18,21,25,26] Decreased CAR expression has also been shown in tumor tissues after repeated injection of Ad-p53.[27,28] It is therefore necessary to assess the CAR expression level of target tumor tissues before and after Ad5-based cancer gene therapy and oncolytic virotherapy.

There are some conventional methods for evaluation of the CAR expression level in tumor tissues, such as flow cytometry, immunohistochemistry, western blotting and reverse transcription (RT)-PCR. Flow cytometry is mainly used to detect CAR-positive human tumor cell lines.[13,24,28,29] Immunohistochemistry is frequently used to assess CAR expression in various human tumor tissues.[11,14,20,23,25] Western blotting is usually performed to confirm the expression of many types of proteins including CAR in molecular biological experiments. Quantitative RT-PCR is also a useful method for evaluation of the mRNA expression of CAR.[18,22] Although these conventional methods can detect CAR expression in tumor tissues, it still remains unclear whether Ad5-based vectors really infect target tumor cells through binding with the CAR that is detected using conventional methods. Therefore, the development of a novel method for assessment of the level of expression of functional CAR in tumor tissues, which is what the Ad5-based vectors really bind, is required for Ad5-based anticancer therapy.

We previously developed a telomerase-specific replication-competent adenovirus OBP-301 (Telomelysin, Oncolys BioPharma, Inc., Tokyo, Japan) that drives the *E1A* and *E1B* genes under the human telomerase reverse transcriptase (*hTERT*) promoter.[8,29–31] OBP-301 infects both normal and tumor cells that express CAR, but replicates only in CAR-positive tumor cells in a telomerase-dependent manner. Furthermore, we recently generated a green fluorescent protein (GFP)-expressing telomerase-specific replication-

[1]Department of Orthopaedic Surgery, Okayama University Graduate School of Medicine, Dentistry and Pharmaceutical Sciences, Okayama, Japan; [2]Center for Gene and Cell Therapy, Okayama University Hospital, Okayama, Japan; [3]Department of Gastroenterological Surgery, Okayama University Graduate School of Medicine, Dentistry and Pharmaceutical Sciences, Okayama, Japan; [4]Department of Medical Materials for Musculoskeletal Reconstruction, Okayama University Graduate School of Medicine, Dentistry and Pharmaceutical Sciences, Okayama, Japan and [5]Oncolys BioPharma, Inc., Tokyo, Japan. Correspondence: Professor T Fujiwara, Department of Gastroenterological Surgery, Okayama University Graduate School of Medicine, Dentistry and Pharmaceutical Sciences, 2-5-1 Shikata-cho, Kita-ku, Okayama 700-8558, Japan.
E-mail: toshi_f@md.okayama-u.ac.jp
Received 15 July 2011; revised 7 November 2011; accepted 5 December 2011; published online 12 January 2012